

NATIONAL HIGH MAGNETIC FIELD LABORATORY

# REPORTS

VOLUME 12 • NO. 1 • 2005

Reviewing the

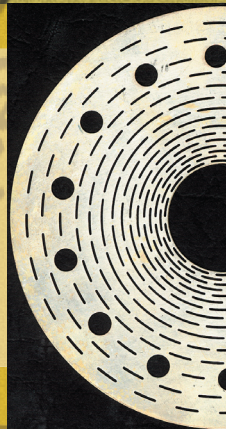
# 2004

# NHMFL RESEARCH REPORTS

**Life Sciences  
Chemistry  
Magnet Science & Technology  
Condensed Matter**

**10 YEARS OF  
FLORIDA-BITTER  
MAGNET TECHNOLOGY**

*Page 35*



# NHMFL REPORTS

## C O N T E N T S

- 3**  
**DEAR READERS**
- 4**  
**LIFE SCIENCES**  
Biochemistry and Biology
- 9**  
**CHEMISTRY**  
Chemistry, Magnetic Resonance  
Techniques, and Geochemistry
- 14**  
**MAGNET SCIENCE &  
TECHNOLOGY**  
Engineering Materials, Instrumentation,  
and Magnet Technology
- 22**  
**CONDENSED MATTER**  
Kondo/Heavy Fermions, Magnetism  
& Magnetic Materials, Metal-Insulator  
Transitions, Molecular Conductors,  
Other Condensed Matter, Quantum  
Fluids and Solids, Semiconductors,  
Superconductivity (Basic & Applied)
- 35**  
**10 YEARS OF  
FLORIDA-BITTER  
MAGNET TECHNOLOGY**
- 38**  
**PEOPLE IN THE NEWS**
- 39**  
**CONFERENCES AND  
WORKSHOPS  
2005**

Published by:  
National High Magnetic Field Laboratory  
1800 East Paul Dirac Drive  
Tallahassee, Florida 32310-3706  
Tel: 850 644-0311  
Fax: 850 644-8350

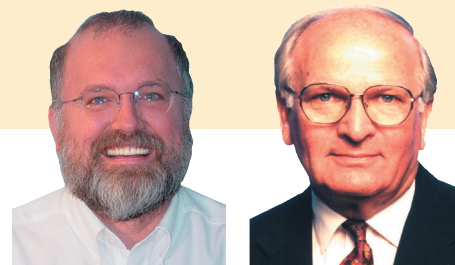
Director: Greg Boebinger  
Editing and Writing: Kathy Hedick  
& Ceci Bell  
Art Direction and Production: Walter Thorner

[www.magnet.fsu.edu](http://www.magnet.fsu.edu)

This document is available in alternate formats upon request. Contact Ceci Bell for assistance. If you would like to be added to our mailing list please write us at the address shown at left, call 850 644-1933, or e-mail [bell@magnet.fsu.edu](mailto:bell@magnet.fsu.edu).



# Dear Readers,



G. Boebinger

R. Schrieffer

Traditionally, the first issue of this newsletter each year is dedicated exclusively to the science and research highlights of the year just ended. This issue, however, will be a little different because we are also marking a very special anniversary:

**10 Years of Florida-Bitter Magnet Technology**, which began on March 18, 1995, when the world's first Florida-Bitter magnet reached its design field of 30 T at the NHMFL in Tallahassee. This magnet was the highest field resistive magnet in the world at that time and quickly became the international standard for high field DC systems. For the full story, see page 35.

We are also diverging somewhat from our traditional approach for featuring the annual science highlights. As part of the redesign of the NHMFL Annual Report, a greater emphasis is being placed on communicating publications, research, and related activities as quickly and as broadly as possible via the laboratory's Web site: [www.magnet.fsu.edu](http://www.magnet.fsu.edu). In November and December, NHMFL users and affiliated faculty submitted brief reports that described their 2004 scientific and R&D activities. All research reports were reviewed and approved by facility and department directors. During January and February, a panel was convened to select Highlights. This year's panel was co-chaired by Chief Scientist J. Robert Schrieffer and NHMFL Director Greg Boebinger, and their first decision was to change the selection strategy. Rather than identifying one highlight for each of 17 or 18 categories, it was decided to collapse the categories into 4 broader groups, thereby allowing greater flexibility in the selections.

Category	Number of Reports Received	Number of Highlights Selected
<b>Life Sciences</b> <i>including Biochemistry and Biology</i>	<b>56</b>	<b>4</b>
<b>Chemistry</b> <i>including Chemistry, Magnetic Resonance Techniques, and Geochemistry</i>	<b>74</b>	<b>4</b>
<b>Magnet Science &amp; Technology</b> <i>including Engineering Materials, Instrumentation, and Magnet Technology</i>	<b>42</b>	<b>7</b>
<b>Condensed Matter</b> <i>including Kondo/Heavy Fermions, Magnetism &amp; Magnetic Materials, Metal-Insulator Transitions, Molecular Conductors, Other Condensed Matter, Quantum Fluids and Solids, Semiconductors, Superconductivity (Basic &amp; Applied)</i>	<b>163</b>	<b>10</b>

Following a comprehensive review of all reports, the panel selected 25 Highlights for 2004 that showcase the broad scientific and technology activities underway at NHMFL facilities at Florida State University, at the University of Florida, and at Los Alamos National Laboratory. Consideration was also given to balancing internal and external activities, and publication status. We are pleased to feature these research reports in this issue of the newsletter and accompany each one with a brief general statement about its significance.

Drs. Schrieffer and Boebinger were extremely impressed with the strength and breadth of the 2004 research reports and remarked how difficult it was to identify the annual Highlights. Readers are strongly encouraged to refer to the Web site for other reports of interest.

Alex Lacerda  
NHMFL Associate Director of User Operations

# LIFE SCIENCES

**M**uscle has a tremendous capacity to adapt to changes in its functional demands, as shown by the desired increases in strength and endurance that accompany exercise and training. Muscle also adapts to forced inactivity, such as occurs when a limb is immobilized in a cast. Here, the response is in many ways the opposite of the response to exercise: it undergoes disuse atrophy, which is marked by weakness and early fatigue. Relative to exercise, however, less is known about the biochemical and metabolic changes in muscle that are associated with disuse atrophy. Using  $^{31}\text{P}$  NMR spectroscopy, Vandeborne and coworkers have investigated the *in vivo* aerobic capacity of muscle in an animal model of disuse atrophy. The time-course of change in phosphocreatine (PCr) of muscle after a bout of stimulation or ischemia is a sensitive measure of *in vivo* aerobic capacity. In this report, Parthare *et al.* find that the time-course of recovery in PCr is significantly slower in the atrophy model, which indicates that immobilization and disuse of muscle are accompanied by a loss of aerobic capacity and mitochondrial function. This has practical implications when considering that disuse atrophy and detraining are common factors following prolonged inactivity associated with many surgeries, heart failures and aging.

## $^{31}\text{P}$ MAGNETIC RESONANCE SPECTROSCOPY OF MOUSE SKELETAL MUSCLE FOLLOWING HIND LIMB CAST IMMOBILIZATION

Parthare, N. (UF, Physical Therapy), Liu, M. (UF, Physical Therapy), Stevens, J.E. (UF, Physical Therapy), Walter, G.A. (UF, Physiology and Functional Genomics), Vandeborne, K. (UF, Physical Therapy)

### Introduction

Apart from structural and morphological adaptations, disuse atrophy has been shown to induce important metabolic adaptations in the skeletal muscle. A large number of *in vitro* studies have shown that there is a significant reduction in the maximal activity of essential oxidative enzymes following immobilization. The purpose of this study was to determine the impact of disuse atrophy on the *in vivo* oxidative capacity of mouse hindlimb muscles using  $^{31}\text{P}$  MRS.

### Methods

The lower hindlimbs of young adult mice (C57BL6 female,  $n = 8$ ) were studied prior to and after 2 weeks of immobilization.  $^{31}\text{P}$  NMR data were acquired in a Bruker 11T spectrometer using a 6-mm x 12-mm oblong  $^{31}\text{P}$  surface coil, placed over the belly of the gastrocnemius muscles. A 3-cm  $^1\text{H}$  surface coil was placed underneath the hindlimb to adjust magnetic field homogeneity.

An inflatable blood pressure cuff was positioned around the animal's thigh. Spectra were collected with a 50  $\mu\text{s}$  square pulse, a TR of 2 s, sweep width of 10,000 Hz and 8,000 complex data points in 30 s bins starting at rest (10 min), during ischemia (30 min), and throughout recovery (30 min). Areas of the resting  $\gamma$ -ATP, inorganic phosphate ( $\text{P}_i$ ), and phosphocreatine (PCr) peaks were determined using area integration following saturation correction. Dynamic changes in PCr levels were determined using complex principal component analysis. The pseudo-first-order rate constant for PCr recovery ( $k_{\text{PCr}}$ ) was determined and used to calculate the *in vivo* oxidative capacity.

### Results and Discussion

Following immobilization, resting  $^{31}\text{P}$  MRS spectra were characterized by a significant increase in the basal  $\text{P}_i$  content ( $\sim 70\%$ ;  $p < 0.001$ ) and the resting  $\text{P}_i/\text{PCr}$  ratio ( $\sim 80\%$ ;  $p < 0.001$ ). The resting PCr content and the intracellular pH values were not different. During 30 minutes of ischemia, the PCr levels decreased by 45 to 55% while the ATP and pH values remained unchanged in both pre immobilized and immobilized muscles. No significant difference was noted in the rate of PCr depletion between pre immobilized versus immobilized muscles ( $0.45 \pm 0.03 \text{ mM/min}^{-1}$  vs.  $0.52 \pm 0.01 \text{ mM/min}^{-1}$ ;  $p = 0.78$ ). In contrast, immobilization induced a 30% decrease in the PCr recovery rate constant ( $0.45 \pm 0.01 \text{ min}^{-1}$  vs.  $0.31 \pm 0.01 \text{ min}^{-1}$ ;  $p < 0.001$ ; Fig. 2). This decrease in  $k_{\text{PCr}}$  reflects a decrease in the *in vivo* oxidative capacity of 5.4 mM ATP/min ( $\sim 35\%$ ).



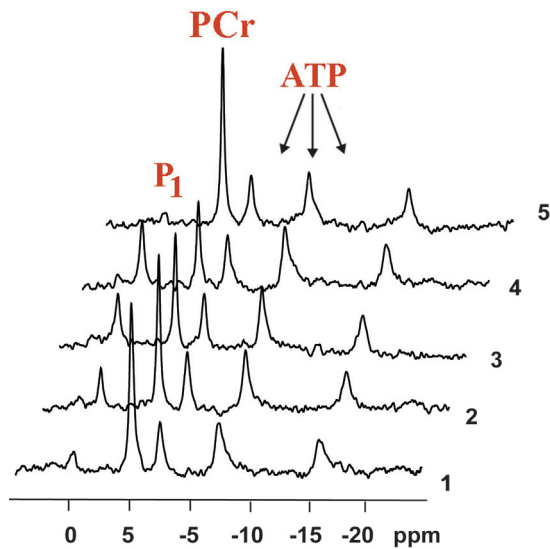


**Figure 1.**  $^{31}\text{P}$  spectra obtained from a pre-immobilized C57 mouse at rest (1), after 10, 20, 30 min of ischemia (2-4) and after 10 min of recovery (5).

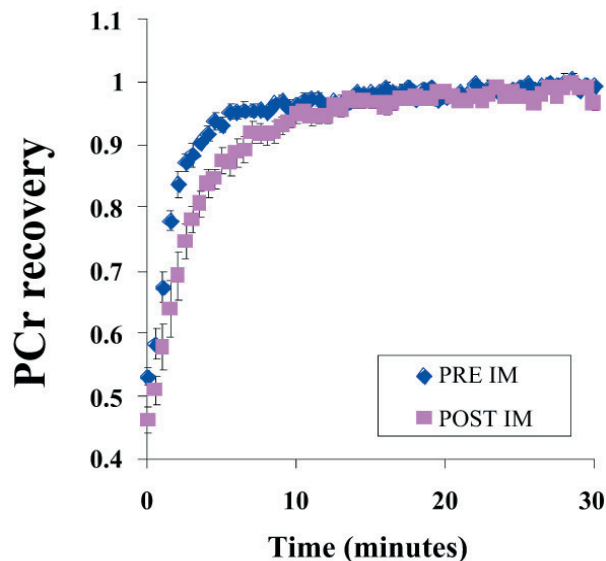


**Figure 2.** PCr recovery kinetics in C57 mice ( $n=8$ ) prior to immobilization (PRE IM) and following 2 weeks of immobilization (POST IM).

## Conclusions

Based on the PCr recovery kinetics following ischemia we conclude that disuse atrophy induces a significant decrease in the *in vivo* oxidative capacity of skeletal muscle. Therefore therapeutic interventions following prolonged inactivity should include strategies to enhance mitochondrial function.

## Acknowledgements

This research was supported by NIH-RO1HD37645, NIH-RO1HD40850. NMR data were obtained at the Advanced Magnetic Resonance Imaging and Spectroscopy (AMRIS) facility in the McKnight Brain Institute of the University of Florida.

**Genetic disorders of mitochondria, the “power plant of the cell,” have been linked to more than forty diseases such as Alzheimer’s, diabetes, Parkinson’s, and cancer. One of the most significant obstacles in treating mitochondrial disorders is that the diagnosis often must rely on indirect and relatively nonspecific markers of metabolism. Simpson and coworkers describe a significant advance in the diagnostic toolkit: using fibroblast cultures, derived from a relatively simple skin biopsy, they performed extracts of their intracellular milieu and examined them with high-field NMR spectroscopy. Mitochondria carry out a complex network of metabolic reactions that can be investigated with the aid of  $^{13}\text{C}$  labeled glucose. Use of  $^{13}\text{C}$  and  $^{31}\text{P}$  NMR spectroscopy permits the quantitative assessment of reaction products and reactants as well as flux through metabolic pathways. In turn, this information permits the locus of metabolic dysfunction to be identified and may lead to making diagnosis of mitochondrial disorders more rapid, specific, and direct.**

## PROBING MITOCHONDRIAL DISORDERS BY NMR SPECTROSCOPY

N.E. Simpson (UF, Medicine), J. Oca-Cossio (UF, Medicine), Z. Han (UF, Medicine), P.W. Stacpoole (UF, Medicine), I. Constantinidis (UF, Medicine)

## Introduction

The traditional approach to diagnosing inborn errors of metabolism has relied on: (1) clinical suspicion of a disease phenotype, (2) quantitation of readily measurable, but relatively nonspecific, surrogate disease markers such as the blood lactate concentration, and (3) enzymological and/or molecular genetic techniques to

identify the primary defect. Very little is known, however, of the quantitative or qualitative consequences of such defects on vital processes, such as the flux through the tricarboxylic acid cycle or the overall intracellular energy charge. Our long-term objective is to investigate the biochemical consequences of primary genetic defects of mitochondrial function. Experiments performed in this study are designed to establish the utility of alginate encapsulation to maintain mitochondrial defective human fibroblasts viable for prolonged periods of time.

## Experimental

Human fibroblasts obtained from skin biopsy samples of patients with mitochondrial defects were cultured and examined by  $^{13}\text{C}$  and  $^{31}\text{P}$  NMR spectroscopy following exposure to uniformly labeled  $^{13}\text{C}$ -glucose for 20 hours prior to a dual phase extraction. Cells were examined in the presence and absence of dichloroacetate (DCA) treatment. All NMR spectra were acquired at 11.75 T vertical bore Bruker Avance-500 spectrometer located at the AMRIS facility of UF. Isotopomer analysis of the glutamate resonances was used to assess relative fluxes through the TCA cycle.

## Results and Discussion

To date we have examined 5 patients with an E1 $\alpha$  defect and one patient with an E1 $\beta$  defect. In addition to these patient samples we have also examined fibroblasts obtained from 5 healthy volunteers.  $^{31}\text{P}$  NMR spectra acquired from the aqueous phase of the extract show that the ATP/ADP ratio was statistically reduced in the E1 $\alpha$  patient population. Analysis of the  $^1\text{H}$  decoupled  $^{13}\text{C}$  NMR spectra (Figure 1) with a Wilcoxon signed rank test determined that the labeled pyruvate pool increased while the flux through pyruvate carboxylase compared to pyruvate dehydrogenase decreased with DCA treatment.

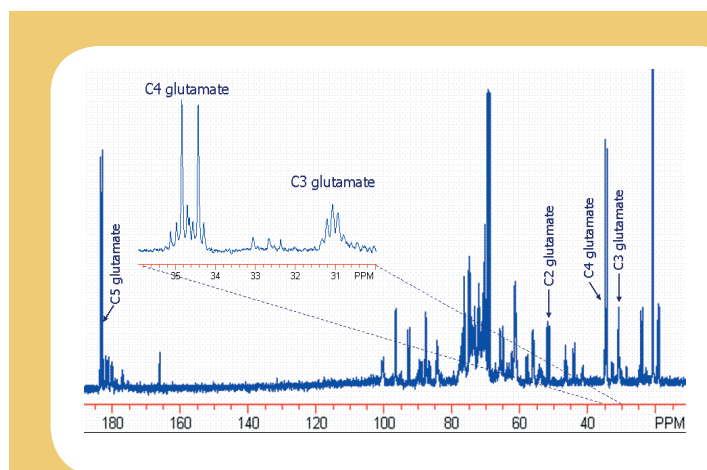


**Figure 1.**  $^1\text{H}$  decoupled  $^{13}\text{C}$  NMR spectrum of human fibroblasts obtained from a patient with an E1 $\alpha$  defective pyruvate dehydrogenase complex.

## Conclusions

Our data show that treatment with DCA increased the energy charge of the E1 $\alpha$  defective cells and altered TCA cycle flux.

Specifically,  $^{13}\text{C}$  NMR spectra showed that the activity of pyruvate carboxylase was markedly reduced and that the cells favored the pyruvate dehydrogenase pathway. Thus, NMR spectroscopic techniques applied to cellular extracts of fibroblast cultures is a useful technique to study the biochemical consequences of inborn errors of metabolism.

## Acknowledgements

This work was supported by NIH grants DK556890 and DK47858. This financial support is greatly appreciated.

**The effects of influenza can range from an annoyance to a life-challenging illness. One of the primary challenges in combating the pathogenicity of the influenza virus, and to developing effective preventative programs and treatments for it, is to understand the mechanisms by which the virus takes over its host cells. An important step in the process of infection involves creation of specific protein channels that permit ions to flow across the membrane systems of the host cell. This work addresses M2, which is a key viral channel protein. Structural resolution by NMR is improved at higher field strengths because the spectra that form the foundation for structural analysis have greater resolution and signal-to-noise. In this study, use of the 900 MHz Ultra Wide Bore NMR Spectrometer at the NHMFL has led to a significant advance in understanding the structure of this viral protein.**

## STRUCTURAL CHARACTERIZATION OF THE M2 PROTON CHANNEL FROM INFLUENZA A VIRUS IN DETERGENT MICELLES BY SOLUTION NMR SPECTROSCOPY AT 900 MHz

M. Sharma (NHMFL/FSU, Chemistry and Biochemistry); F.P. Gao (NHMFL/FSU, Chemistry and Biochemistry); K.K. Shetty (NHMFL/FSU); W.W. Brey (NHMFL/FSU); R. Fu (NHMFL/FSU), T.A. Cross (NHMFL/FSU, Chemistry and Biochemistry)



Influenza A virus, like other enveloped viruses, enters the host by attaching to the host cell's membrane. Membrane fusion which is triggered by conformational changes of the membrane protein hemagglutinin and the release of the virus' RNA into the host cell are consequences of lowering of the pH. M2 protein of influenza A virus forms a homo-tetrameric proton channel that is involved in modifying virion and trans Golgi pH for virus infection. The protein is 97 residues long with a 19 residue long transmembrane helix. This homo-tetrameric assembly is activated at low pH and inhibited by influenza drugs amantidine and rimantidine. M2 protein is a potential paradigm system for the functional and structural studies of viral ion channels. Three dimensional structure of 25 residue long peptide including transmembrane helix was solved by our group using solid state NMR<sup>1</sup>. But the structure and functional analysis of the full-length M2 protein still remains elusive. The efforts in this direction are underway using solid and solution state NMR spectroscopy and combination thereof. We here report initial solution NMR results for full length M2 protein.

M2 protein was cloned, expressed, and purified with uniform <sup>15</sup>N, <sup>15</sup>N/<sup>13</sup>C and amino acid specific <sup>15</sup>N-Leu, <sup>15</sup>N-Phe and <sup>15</sup>N-Trp labeling. The yield for purified protein varied from 30 mg/Liter for <sup>15</sup>N/<sup>13</sup>C to 150 mg/Liter <sup>15</sup>N-Phe labeled M2 protein. The preliminary requirement of structural and functional studies of proteins is to complete resonance assignments which (more specifically for membrane proteins than for soluble proteins) are in turn dependent upon successful determination of optimum condition for NMR sample preparation. A considerable time and effort were spent to obtain the optimum combination of pH, detergent type and detergent concentration to keep the characteristic line-broadening tractable while keeping the protein in best possible native-like environment. Fig. 1 shows the (<sup>15</sup>N-<sup>1</sup>H)-TROSY spectra obtained for 1 mM M2-protein in detergent micelles at 720 MHz Varian Spectrometer and 900 MHz Ultra Wide Bore Spectrometer. Both spectra were acquired with 32 scans and 256 increments in the indirect dimension. Due to significantly higher resolution and signal-to-noise ratio achieved on 900 MHz spectrometer, 90% of the total number of expected peaks could be identified.

### Acknowledgements

The work was supported by NIH and NHMFL.

### References

- 1 Wang, J., *et al.*, Prot. Sci., **10**, 2241-2250 (2001).

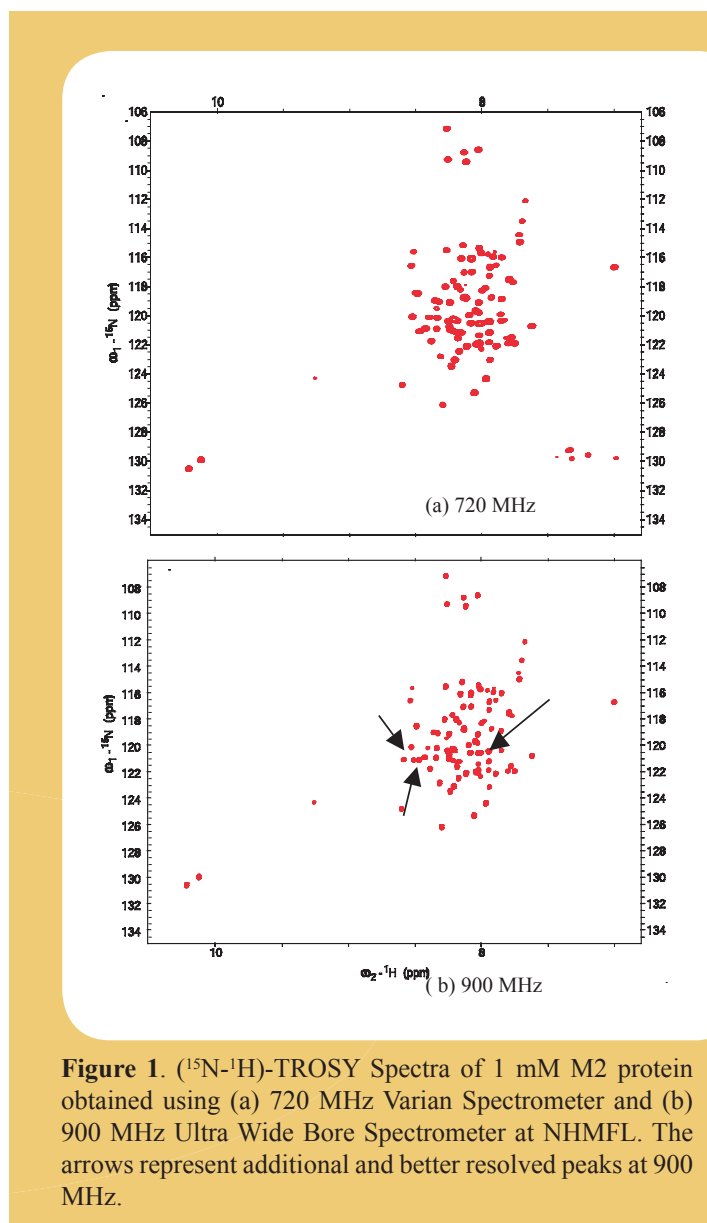


**Figure 1.** (<sup>15</sup>N-<sup>1</sup>H)-TROSY Spectra of 1 mM M2 protein obtained using (a) 720 MHz Varian Spectrometer and (b) 900 MHz Ultra Wide Bore Spectrometer at NHMFL. The arrows represent additional and better resolved peaks at 900 MHz.

**The active agent in the AIDS-causing human immunodeficiency virus (HIV) is RNA. Outside a cell, the RNA is packaged in a protein “capsid.” After the virus enters a human cell, the main protein of the capsid is cut into several pieces, one of which (CA, ~24,000 Dalton in mass) spontaneously assembles into hexamers that interlock to form a sort of mesh that envelops and protects the virus. Thus, an obvious drug target is the contact surface between adjacent CA molecules—once those contact sites are known, one can imagine designing a drug to bind there, thereby destroying the mesh and leaving the RNA unprotected. Last year, the NHMFL ICR group was able to locate the contacts between CA hexamers by dissolving them in heavy water (D<sub>2</sub>O). As each surface-exposed CA protein backbone -NH hydrogen is replaced by deuterium, the mass goes up by 1 Dalton. Thus, by**

letting the H/D exchange proceed for a while, then cutting up the protein into pieces and weighing them by FT-ICR mass spectrometry, it was possible to determine which parts of the protein were exposed to the solvent. The contact sites could then be identified as those segments that are solvent-inaccessible in the hexamer but not in the monomer. This year, the group was able to repeat the experiment with intact capsids. The results were the same, except that only half of the CA molecules self-assemble to form the hexameric mesh network under these more biologically realistic conditions. In support of that finding, independent experiments have recently shown that mutations at this hexamer interface result in non-infective virus particles. Finally, these results were obtained for a system for which neither X-ray diffraction nor NMR was possible—a good example of how mass spectrometry can contribute to the arsenal of powerful bioanalytical tools.

### KEY INTERACTIONS IN HIV-1 MATURATION IDENTIFIED BY HYDROGEN-DEUTERIUM EXCHANGE

Jason Lanman (U. of Alabama-Birmingham, Microbiology), TuKiet T. Lam (NHMFL/FSU, Chemistry and Biochemistry), Mark R. Emmett (NHMFL/FSU, Chemistry and Biochemistry), Alan G. Marshall (NHMFL/FSU, Chemistry and Biochemistry), Michael Sakalian (U. of Oklahoma Health Science Center) and Peter E. Prevelige, Jr. (U. of Alabama-Birmingham, Microbiology)

### Introduction

To characterize the intersubunit interactions underlying assembly and maturation in HIV-1, we determined the amide hydrogen exchange protection pattern of capsid protein (CA) in the immature virion and the mature virion by FT-

ICR mass spectrometry. Alterations in protection upon maturation provide evidence for the maturation-induced formation of an interaction between the N- and C-terminal domains in half of the capsid molecules, indicating that only half of the capsid protein is assembled into the conical core.<sup>1</sup>

### Results and Discussion

H/D-exchanged immature and mature virus-like particles (iVLP and mVLP) were digested with pepsin and the extent of deuterium incorporation into each peptide was analyzed by high resolution mass spectrometry. The peptide spanning CA residues 55 to 68 (m/z 744.84) corresponding to the N/C interface identified *in vitro*<sup>1</sup> displays a bimodal distribution in the mature virion but not in the immature virion. The H/D exchange profiles of the 55-68 segment in iVLP and the faster component in the bimodal H/D-exchange profile of mVLP are very similar to that seen for unassembled CA,<sup>1</sup> indicating that these CA molecules are probably similar in conformation to CA from unassembled subunits. The exchange profile for the slower exchanging component in mVLP is similar to that previously observed for *in vitro* assembled CA,<sup>1</sup> suggesting that the core associated CA molecules form the heterotypic N-terminal domain:C-terminal domain interaction in mVLP. The relative distribution of fast and slow exchanging subpopulations agrees well with that observed in intact CA and suggests this interface is present in the bulk of the core associated molecules independent of their location.

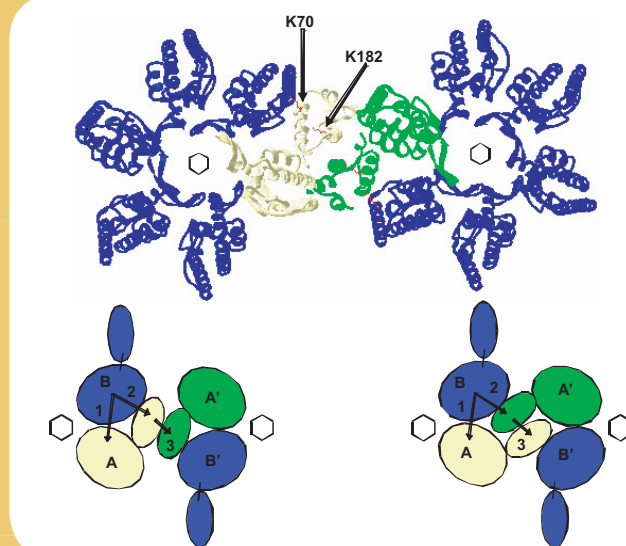


**Figure 1.** Top: Hexamer-hexamer CA protein interaction sites (K is lysine). Bottom: The ICR experiments narrow the possible configurations to the two shown here.

Taken together, the present results suggest that helices I and II are involved in intersubunit interactions in both the immature and mature virion, whereas a defining characteristic of core formation appears to be the formation of the heterotypic N-terminal domain:C-terminal domain interaction. In support of this model, mutations in this interface region result in non-infectious virions, and a small molecule compound that binds near the interface interferes with core formation but not assembly.



## Acknowledgements

This work was supported by grants from the U.S. National Institutes of Health (AI44626) and the U.S. National Science Foundation (CHE-99-09502), Florida State University, and the U.S. National High Magnetic Field Laboratory.

## References

- 1 Lanman, J., *et al.*, *J. Mol. Biol.*, **325**, 759-772 (2003).
- 2 Lanman, J., *et al.*, *Nat. Struct. Mol. Biol.*, **11**, 676-677 (2004).

# CHEMISTRY

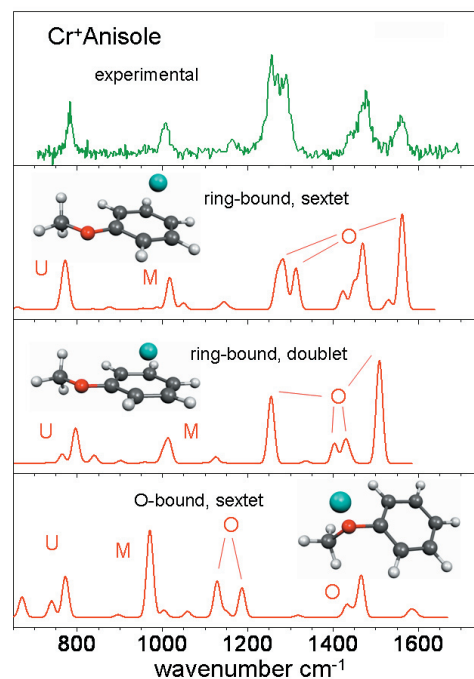
In this international collaboration, an FT-ICR instrument was built at U.F. and then interfaced to a free electron laser in The Netherlands. That system is now available to users worldwide. The graphic clearly shows how to identify the correct structure of a gas-phase ion by comparing the experimental IR spectrum to normal mode mid-IR spectra for each of various putative structures. Last year's highlight in this category was from NMR. It's nice to rotate from year to year.

## GAS-PHASE $\text{Cr}^+$ COMPLEXES OF AROMATIC LIGANDS: SITE OF BINDING AND SPIN STATE OF THE METAL ION CHARACTERIZED BY INFRARED SPECTROSCOPY USING THE FELIX FREE-ELECTRON LASER

R.C. Dunbar (Case Western Reserve U., Chemistry); J. Oomens (FOM Institute); D. T. Moore (FOM Institute); G. von Helden (Fritz-Haber-Institut der Max-Planck-Gesellschaft); G. Meijer (Fritz-Haber-Institut der Max-Planck-Gesellschaft); J. R. Eyler (UF, Chemistry)

### Introduction

The combination of a Fourier-transform ion cyclotron resonance (FT-ICR) spectrometer with the Free Electron Laser for Infrared eXperiments (FELIX) at FOM Institute in Nieuwegein, Netherlands<sup>1</sup> has been found to give remarkable new capabilities for characterizing gas-phase organometallic complexes of transition metal ions. In initial work described in the *2003 NHMFL Research Review* (Dunbar, R.C., *et al.*, p. 76) and subsequently published<sup>2</sup> it was found that the site of binding of the  $\text{Cr}^+$  ion to a bi-functional ligand (aniline) could be identified



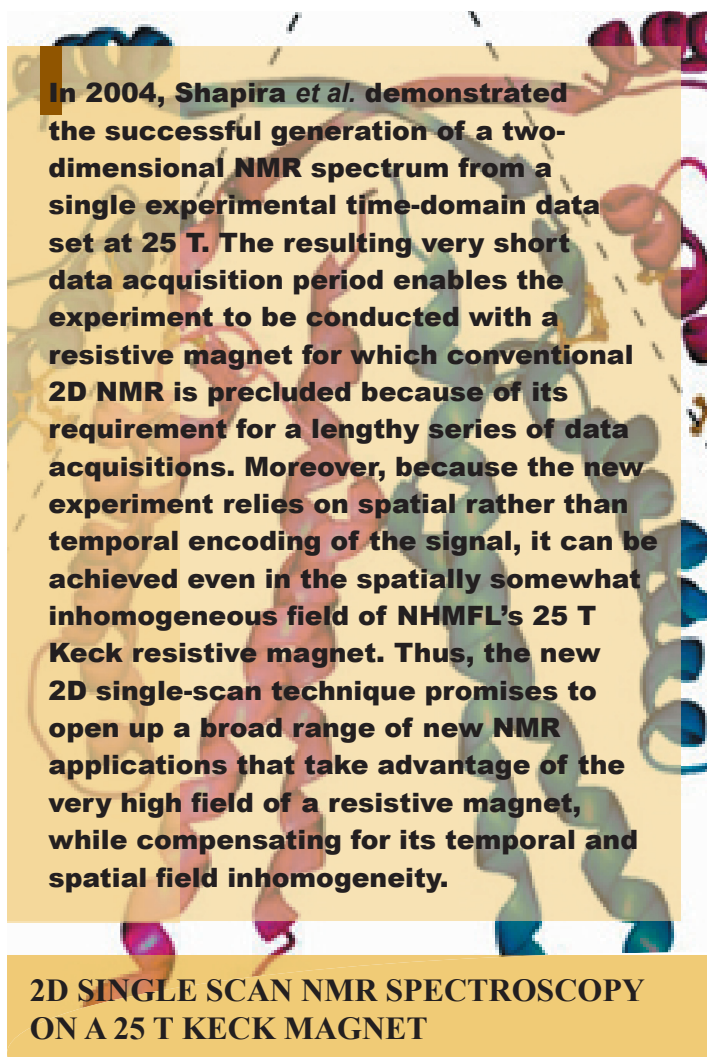
with confidence. In new work including additional ligands (anisole, acetophenone) it has been shown that not only the site of complexation, but also the spin state of the metal ion can be identified.

## Experimental

The FELIX laser provides continuously tunable IR radiation over the IR fingerprint region, typically 10 macropulses of pulse energy 35 mJ. Light is directed into the cell of the FT-ICR spectrometer (4.7 T actively shielded magnet). Atomic metal ions are produced external to the magnet by laser desorption/ionization, and guided into the cell. Organometallic complexes are formed by ion chemical processes within the cell, isolated by selective ion ejection, and their signal intensity is monitored both with and without FELIX irradiation to determine dissociation rate versus wavelength.

## Results and Discussion

The figure shows the results for anisole, as an example. In the top panel is shown the infrared photodissociation spectrum from the FT-ICR/FELIX instrument. The other panels show the computed predictions for high-spin ring-bound, low-spin ring-bound, and high-spin side-chain-bound complexes. The high-spin ring-bound prediction clearly gives by far the best fit to the experiment.



**In 2004, Shapira *et al.* demonstrated the successful generation of a two-dimensional NMR spectrum from a single experimental time-domain data set at 25 T. The resulting very short data acquisition period enables the experiment to be conducted with a resistive magnet for which conventional 2D NMR is precluded because of its requirement for a lengthy series of data acquisitions. Moreover, because the new experiment relies on spatial rather than temporal encoding of the signal, it can be achieved even in the spatially somewhat inhomogeneous field of NHMFL's 25 T Keck resistive magnet. Thus, the new 2D single-scan technique promises to open up a broad range of new NMR applications that take advantage of the very high field of a resistive magnet, while compensating for its temporal and spatial field inhomogeneity.**

**2D SINGLE SCAN NMR SPECTROSCOPY ON A 25 T KECK MAGNET**

Boaz Shapira, [Lucio Frydman](#) (Weizmann Institute, Israel); Zhehong Gan (NHMFL, CIMAR/NMR)

Among these three ligands, ring binding has been proven for anisole and aniline, while acetophenone binds at the oxygen. The bis-complexes of aniline and anisole were shown to be low-spin, whereas the respective mono-complexes, as well as the acetophenone bis-complex, are high-spin.

## Acknowledgements

Establishment of the FT-ICR facility at FELIX was made possible by funding (NSF #CHE-9909502) from the NHMFL. This work was financially supported by the Nederlandse Organisatie voor Wetenschappelijk Onderzoek (NWO). RCD acknowledges the support of the donors of the Petroleum Research Fund, administered by the American Chemical Society.

## References

- 1 van Heijnsbergen, D., *et al.*, *J. Am. Chem. Soc.*, **124**, 1562-63 (2002).
- 2 Oomens, J., *et al.*, *J. Am. Chem. Soc.*, **126**, 724-25 (2004).

## Introduction

2D NMR involves scanning a series of time-domain signals  $S(t_2)$  as a function of a  $t_1$  time variable which undergoes parametric incrementation throughout independent experiments. This procedure requires, first and foremost, a stable NMR magnet that does not change during the course of the acquisition. Therefore, in spite of their unique strengths, the relatively unstable Bitter magnet design does not provide the sufficient stability demanded by 2D NMR acquisitions—they are qualified for the execution of only a single scan experiment. High inhomogeneities constitute a related issue from which Bitter magnets suffer, as they result in low spectral resolution which makes it difficult to resolve inequivalent sites. Very recently, the Frydman laboratory originated a general approach whereby the serial data acquisition mode of 2D NMR can be parallelized, enabling the acquisition of complete multi-dimensional NMR data sets within a single transient. The short timescale of such “ultrafast” 2D experiments should enable us to overcome many of the problems associated with the time instability of the Bitter system. Furthermore, the fact that ultrafast NMR relies on a spatial rather than on a time-domain encoding of the signals could allow us to implement high resolution NMR acquisitions even when using inhomogeneous fields.<sup>2</sup> These two features combined could enable the successful acquisition of high resolution liquids 2D NMR spectra at the intense fields provided by Bitter systems; a natural candidate for exploring this was the NHMFL Keck magnet.

## Experimental

Spectra were measured on the Keck magnet at 25 T using a Tecmag console and Doty probe with a single axis z gradient. Maximum strengths of 90 G/cm and receiver coil lengths of 1 cm long were calibrated prior to the actual measurements on a model 7 T system; 60 Hz  $B_0$  fluctuations were attenuated with a flux stabilizer designed and built by W.W. Brey and coworkers at the NHMFL.



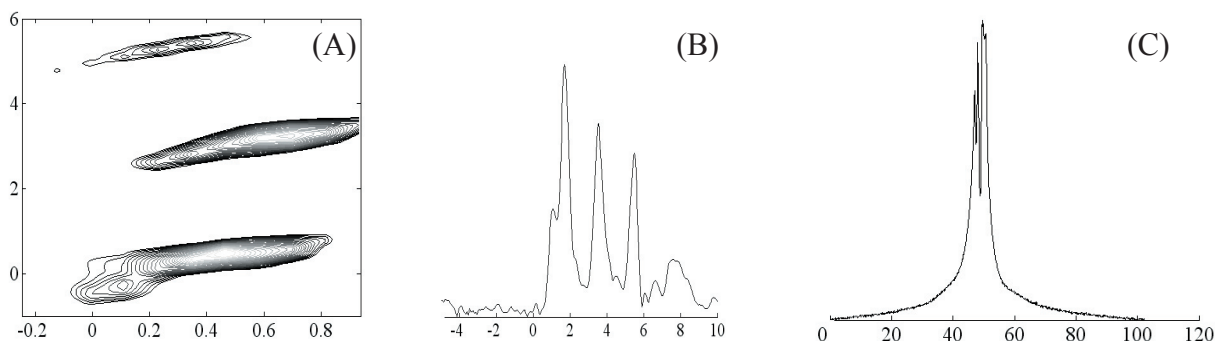


**Figure 1.** (A) Mixing-less  $^1\text{H}$  2D NMR spectrum recorded on 95% EtOH at 21.2 T. (B) Slice extracted from the 2D spectrum, showing the potential for resolving the various sites. (C) Comparable 1D NMR trace arising from the same sample after a single pulse excitation. Spectral axes are given in kHz (C) and in ppm referenced to  $\text{H}_2\text{O}$  (ext.) in (A) and (B).

## Results and Discussion

During 2004, we began exploring ultrafast 2D NMR's potential by implementing a continuous spatial excitation sequence without any mixing period and without extensive compensation for the effects of inhomogeneities. Our principal goal at this stage was to test the overall feasibility of the concept, and the suitability of the NMR hardware available at the NHMFL. Fig 1 shows preliminary results on a 95% ethanol sample, which promises a bright future for the approach exposed above. This molecule exhibits three peaks located at 1.22, 3.6, and 5.4 ppm. As can be seen in Fig. 1C, the inhomogeneity and instability of the Keck system is such that no real resolution of the three sites can be observed in a conventional single-pulse 1D acquisition. By contrast, no complications in distinguishing the three sites are observed upon carrying out even a mixing-less single-scan 2D NMR experiment, where inhomogeneities appear correlated along orthogonal dimensions and thus allow a clear distinction of the peaks. The spectral

width along  $\nu_2$  was in this case only 1.2 ppm, which resulted in peak folding. Still, cross section of the peaks taken from the 2D spectrum provide a first glimpse into the high resolution liquid-state potential of the 25 T system (Fig. 1A): the FWHM are then ca. 5 times smaller than in the single-pulse experiment.

## Conclusions

The prospects for carrying out single-scan high-resolution 2D NMR experiments are excellent. Our main goals during 2005 will be to activate a sample spinning device capable of further reducing linewidths, and to extend the homonuclear 2D experiments tested so far to heteronuclear cases.

## References

- <sup>1</sup> L. Frydman, *et al.*, *J. Am. Chem. Soc.*, **125**, 9204-9217 (2003).
- <sup>2</sup> B. Shapira, *et al.*, *J. Am. Chem. Soc.*, **126**, 7184-7185 (2004).

**In this work, we performed dipolar recoupling experiments at 900 MHz to be used for structural determination. Those experiments clearly demonstrate that the newly available 900 MHz magnet is of high quality in terms of stability and homogeneity and it is capable of conducting a variety of solid state NMR experiments ranging from biological solids and quadrupolar nuclei in materials science. As demonstrated in this report, in addition to sensitivity enhancement, high field greatly improves spectral resolution so as to increase frequency selectivity leading to precise distance measurements, which are the key to accurately elucidating secondary structures of molecules such as proteins and polypeptides in solids.**

## DIPOLAR RECOUPLING NMR SPECTROSCOPY AT 900 MHz

R. Fu (NHMFL); W.W. Brey (NHMFL); T.A. Cross (NHMFL/FSU)

## Introduction

In the initial stage of the 900 commissioning period, scientists at the NHMFL are exploiting a variety of scientific projects that can take advantage of the ultra-wide bore 900 MHz magnet, from

biological solids to quadrupolar nuclei in materials science. Here we used a uniformly  $^{13}\text{C}$ ,  $^{15}\text{N}$  labeled valine sample to demonstrate some dipolar recoupling experiments on 900 MHz, the methods in general used to obtain distance constraints for structure determination.

## Experimental Results

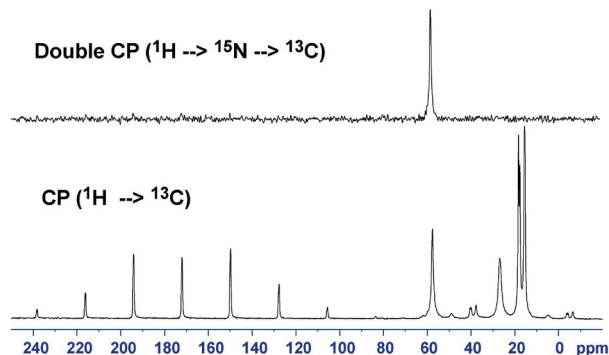


**Figure 1.**  $^{13}\text{C}$  CPMAS spectra of uniformly  $^{13}\text{C}$ ,  $^{15}\text{N}$  labeled valine sample using a 3.2 mm Bruker triple-resonance CPMAS probe. This type of technique has been widely used to acquire 2D  $^{13}\text{C}$ - $^{15}\text{N}$  correlation spectra of uniformly labeled samples. A large chemical shift dispersion at 900 MHz enhances spectral resolution, thus permitting us to more accurately determine structural connectivities of molecules.

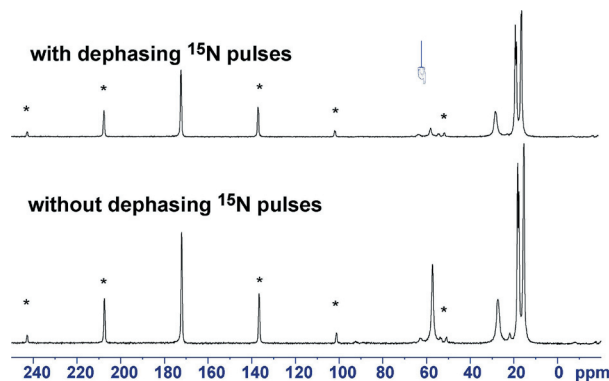


**Figure 2.**  $^{13}\text{C}$  spectra of uniformly  $^{13}\text{C}$ ,  $^{15}\text{N}$  labeled valine sample using a 3.2 mm Bruker triple-resonance CPMAS probe. The asterisks indicate spinning sidebands. From the changes in  $^{13}\text{C}$  signal intensities vs. the dephasing time, we can precisely measure internuclear distances between the  $^{13}\text{C}$  and  $^{15}\text{N}$  sites. Distance constraints, along with orientational constraints and torsional constraints, lead to secondary structural determination of proteins and polypeptides.<sup>1,2</sup>

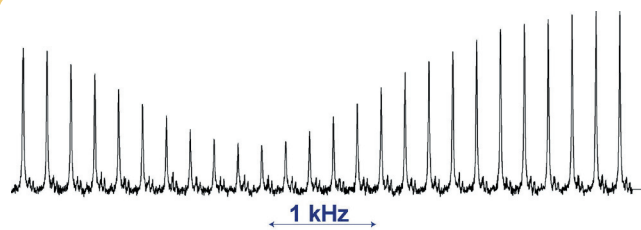


**Figure 3.** Plot of  $^{15}\text{N}$  dephased  $^{13}\text{C}$  spectra of the valine sample vs.  $^{15}\text{N}$  offsets. Here only the signal at 57 ppm is shown. At on-resonance the  $^{13}\text{C}$  signal is efficiently dephased by the  $^{15}\text{N}$  pulses, while at off-resonance, the dephasing becomes insufficient. Frequency-selective heteronuclear recoupling<sup>3</sup> allows one to select a spin-pair in uniformly labeled samples thus to measure their internuclear distance without interference from other labeled sites. A large chemical shift dispersion at 900 significantly increases the frequency selectivity.

## References

- 1 Gullion, T., *et al.*, *J. Magn. Reson.*, **81**, 196 (1988).
- 2 Fu, R., *et al.*, *Chem. Phys. Lett.*, **272**, 361-369 (1997).
- 3 Bennett, A.E., *et al.*, *J. Chem. Phys.*, **100**, 812 (1994).

**T**he research reported on shows that part of the Hawaiian plume contains an ancient (older than one billion years) depleted component. The “depleted component” is depleted in trace elements that prefer to reside in melts compared to silicate minerals. Ocean island volcanics in general are characterized by enrichments in trace elements that prefer the melt over solid. This is the first time that such a depleted component is recognized in Hawaii. The research is accepted for publication by *Geochimica Cosmochimica Acta*.



## EVIDENCE FOR A DEPLETED COMPONENT IN HAWAIIAN VOLCANISM FROM HAFNIUM-NEODYMIUM ISOTOPE SYSTEMATICS OF GARNET PYROXENITES

M. Bizimis (FIU, Earth Sciences/NHMFL, Geochemistry), G. Sen (FIU, Earth Sciences), V.J.M. Salters (NHMFL, Geochemistry), S. Keshav, (GL, Carnegie Inst. Washington)

### Introduction

Characteristic of Hawaiian and other oceanic island volcanism is the eruption of small volume, highly alkalic, and incompatible element enriched “post-erosional” lavas at the end of volcano activity. These lavas



are isotopically more depleted than the voluminous tholeiitic, shield-building stage volcanism requiring a trace element enriched, but long term depleted mantle source. The presence of garnet pyroxenite xenoliths in the post erosional lavas from Oahu, Hawaii, provide a unique opportunity to study the deeper (>60 km) lithosphere and the processes taking place therein. Here we present the first comprehensive major, trace element and Hf, Nd, and Sr isotope investigation of clinopyroxene and garnet mineral separates from a set of garnet clinopyroxenite xenoliths from the Salt Lake Crater, Oahu, Hawaii, in order to constrain their origin in the context of Hawaiian volcanism.

### Results and Discussion

Thermobarometric calculations suggest that these SLC garnet pyroxenites last equilibrated at 20 to 30 kb (60 to 90 km) and about 1200 C. These temperatures are about 200 to 300 degrees C hotter than the temperature of the lithosphere at these depths. The calculated melts in equilibrium with these pyroxenites better resemble the Honolulu Volcanics (HV), rather than MORB or EMORB. In terms of Lu-Hf and Sm-Nd isotope systematics, all clinopyroxene-garnet mineral pairs analyzed here show, within error, zero-age. The SLC pyroxenites have relatively radiogenic Hf isotope compositions ( $\epsilon_{\text{Hf}} = 11.8-18$ ), for a given Nd, ( $\epsilon_{\text{Nd}} = 7.2-8.5$ ) and define a distinct steep slope (3.2) in  $\epsilon_{\text{Hf}}-\epsilon_{\text{Nd}}$  isotope space, similar to the Honolulu Volcanics but unlike most other ocean island basalts (OIB). The above evidence suggests that these pyroxenites are zero-age cumulates from melts isotopically similar to the Honolulu Volcanics. However the distinct steep slope in Hf/Nd isotope space of both SLC pyroxenites and HV lavas require an endmember component that falls above the OIB array. Such an endmember is identified in the SLC spinel peridotites that have extremely radiogenic Hf and unradiogenic Os isotope compositions and have been explained as ancient (> 1Ga) depleted recycled oceanic lithosphere<sup>1,2</sup>. However, the radiogenic Os isotope compositions in similar pyroxenites<sup>3</sup> require that such ancient lithosphere cannot directly contribute (directly by melting, or indirectly by reaction) to melts that give rise to the pyroxenites. Instead, melts derived from this depleted lithosphere must mix with a (presumably) plume-derived melt with radiogenic Os isotopic composition to generate these pyroxenites and, by inference based on the similarities, the Honolulu Volcanics. Irrespective of the Os isotopes however, the Hf/Nd isotopes clearly require a previously depleted component to contribute to these pyroxenites.

### Conclusions

The zero-age Lu-Hf, Sm-Nd isotope systematics of the SLC garnet pyroxenites and their Hf-Nd isotope similarity to the host Honolulu volcanics points to a genetic link between the two. The relatively radiogenic Hf isotope ratios require a depleted component, unlike MORB, in the source of these pyroxenites. Whether this depleted lithosphere is an ancient (>1 Ga old) depleted lithospheric component intrinsic to the Hawaiian plume (i.e. recycled old lithosphere) or the 100 Ma old lithosphere that lies beneath Oahu, is not entirely clear. Based on the isotopic similarities between the recent Honolulu volcanics and old (70 Ma) volcanics from the Emperor seamounts, Frey *et al.*<sup>4</sup> suggested that a depleted component, intrinsic to the hot spot, must have been present in the source of both lavas. In this case, we consider it more likely that the depleted component recognized in these pyroxenites resides within the Hawaiian plume and its signature becomes more evident in the winding stage of volcanism where it is not diluted by the voluminous shield-stage plume melts.

### References

- 1 Bizimis, *et al.*, EPSL, **217**, 43-48 (2004).
- 2 Bizimis, *et al.*, AGU, Fall meeting Abstracts (2004).
- 3 Lassiter, *et al.*, EPSL, **178**, 269-284 (2000).
- 4 Frey, *et al.*, G<sup>3</sup> (in press).

# MAGNET SCIENCE & TECHNOLOGY

**R**ecrystallization processes in cold worked metals advance during heat treatment by changes in the microstructure caused by change of average grain size and its orientation distribution. Grain boundary motion is the dominating process. It can be affected by a magnetic field because a driving force is induced due to crystal and shape anisotropy of the susceptibility. Magnetic fields are, therefore, an excellent means to study these effects in ferromagnetic materials and also for materials processing. Earlier experiments of Molodov *et al.* at the NHMFL have shown that grain boundary motion can also be observed in non-ferromagnetic materials if the magnetic field is strong enough. His report on grain growth in Ti by means of magnetic annealing demonstrates that the texture evolution can be effectively influenced. Similar experiments on single Zn crystals show a clear deviation from the random distribution after magnet annealing. In this context, reference is made to the development of a new technique by the same author to measure grain boundary migration *in situ* with a space resolving polarization microscopy probe. This research field has the highly promising potential for future industrial applications that materials can be tailored with magnetic fields to specific needs.

## MAGNETICALLY DRIVEN SELECTIVE GRAIN GROWTH

P.J. Konijnenberg, D.A. Molodov, and G. Gottstein (RWTH-Aachen University, Institute of Physical Metallurgy and Metal Physics)

### Introduction

At suitably high field strengths and temperatures even the microstructure evolution of non-ferromagnetic anisotropic metals is affected by magnetic annealing.<sup>1</sup> During this process the non-uniformity and anisotropy of the boundary mobility plays an important role. Selective grain growth during magnetic annealing yields valuable insight into these parameters.

### Experimental and Results

Large single crystals (2x4x15mm<sup>3</sup>, Zn 99.99+%) were locally deformed by a Vickers hardness indentation along either  $\langle 2110 \rangle$  or  $\langle 1010 \rangle$ . Annealing at about 673 K in a high purity inert gas atmosphere initiated a local recrystallization which resulted in a set of new local orientations. SEM-EBSD analysis revealed that at the sample surface all grains invariably border with the host matrix. Rodrigues-Frank parameters of boundaries between these grains and the single crystalline host matrix are plotted separately; disorientation angles in Fig. 1a and disorientation axes in Fig. 1c. Both figures show a clear deviation from a random distribution (resp. indicated by a MacKenzie distribution and contour lines).

A subsequent addition of a high magnetic field (Keck magnet) for several minutes (in similarly pretreated samples) along the extraordinary axis of the host matrix resulted frequently in selective growth of an individual grain into the single crystalline host



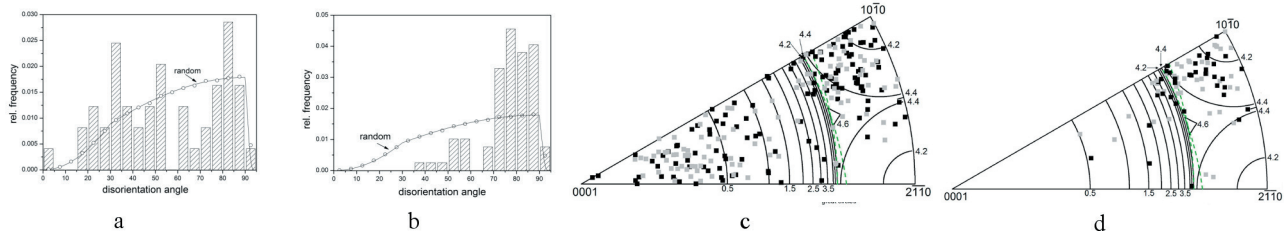


**Figure 1.** Disorientation angle and axis distribution before (a,c) and after (b,d) magnetic annealing.

matrix. Orientations of these grains were determined by Laue X-ray backscatter diffraction. Apparently these grains can be distinguished from their competitors by their combination of driving force and boundary mobility. Boundaries of these prevailing grains are plotted correspondingly in Fig. 1b and d.

## Discussion

Clearly, after magnetic annealing a large part of the angle distribution as available before magnetic annealing is suppressed. The axis distribution behaves similarly. Before magnetic annealing two clusters can be recognized; roughly around  $\langle 0001 \rangle$  and  $\langle 10\bar{1}0 \rangle$  of which only the latter is maintained after magnetic annealing. The angle distribution becomes less random whereas the axis distribution becomes more random, seen along the symmetry line  $\langle 0001 \rangle$ - $\langle 10\bar{1}0 \rangle$ . Due to the sample geometry boundary normals point along  $\langle 0001 \rangle$  of the host matrix. Consequently selectively grown grain boundaries have a strong asymmetric  $\langle 10\bar{1}0 \rangle$  tilt component. Previous research revealed, however, that symmetric  $\langle 10\bar{1}0 \rangle$   $86 \pm 3^\circ$  tilt boundaries tend to be quite immobile under similar conditions. Further research is needed.

## Acknowledgements

Financial support from the Deutsche Forschungsgemeinschaft (GO 335/24) is gratefully acknowledged.

## References

- <sup>1</sup> Molodov, D.A., *et al.*, *Acta Mat.*, **52**, 4377-4388 (2004).

## **IN SITU MEASUREMENTS OF GRAIN BOUNDARY MIGRATION WITH A HIGH MAGNETIC FIELD POLARIZATION MICROSCOPY PROBE**

P.J. Konijnenberg, D.A. Molodov, and G. Gottstein (RWTH-Aachen University, Institute of Physical Metallurgy and Metal Physics)

### Introduction

A space resolving high magnetic field polarization microscopy probe has been developed to track grain boundaries at the surface of magnetically anisotropic metals during magnetic annealing at high field strengths. It is known from experiments that also in non-ferromagnetic anisotropic materials a sufficient driving force for grain boundary migration can be provided by external high magnetic fields.<sup>1,2,3</sup> Two major advantages in this approach to measure boundary properties are a constant, adjustable, and accurately known driving force and the possibility to drive plane grain boundaries with a uniform and well defined boundary structure.

### Experimental and Results

In essence this probe comprises a conventional polar magneto-optic Kerr setup. An incident light polarizing microscope with CCD camera in field direction is arranged over a sample chamber at the field center. The gas tight sample chamber is equipped with

a quartz window and an adjustable DC resistance heated sample stage perpendicular to the field direction. The heater temperature is gauged by two platinum resistance sensors to avoid drift effects on usual thermocouples. The sample temperature is derived from a calibration curve and accurate within 1 K. For lower than cubic crystal symmetries, grain boundaries become visible as a contrast between differently orientated crystallites due to a plane polarized LED-illumination in combination with an analyzing filter in front of the CCD. A spectral half width of 20 to 30 nm enables it to anticipate to a large Faraday rotation of the polarization plane in the field. Microscope images are digitally stored at regular instances. Focus and both polarizing filters are remotely controlled by three DC stepper motors on top of the magnet, 1.4 m off axis. The current configuration was successfully tested at sample temperatures up to 673 K and fields of 25 T in the 50 mm Keck magnet.

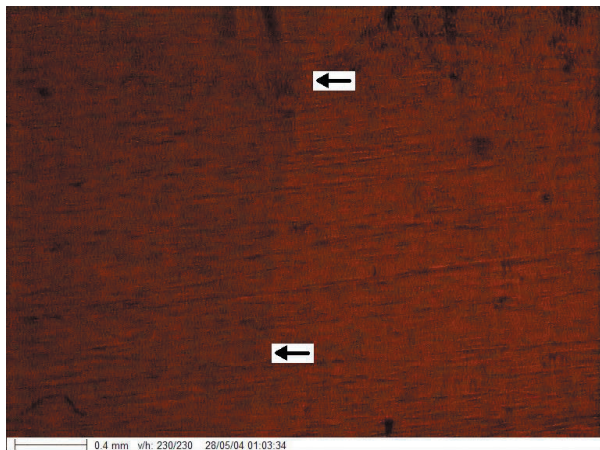
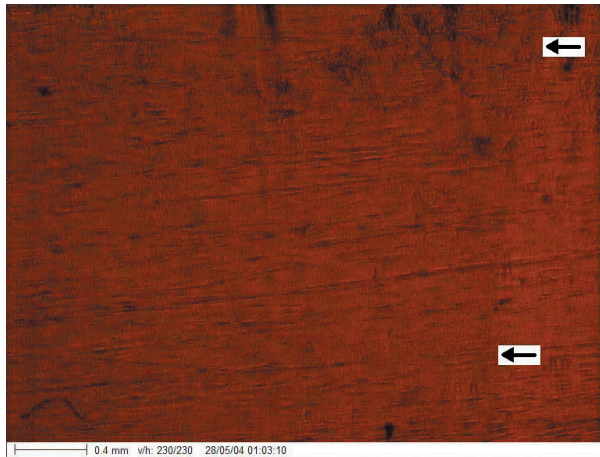
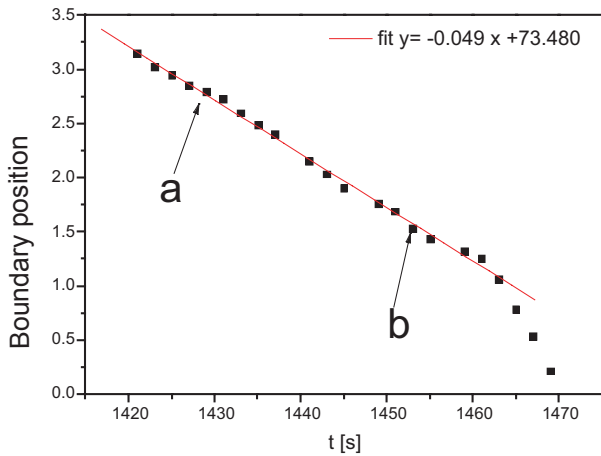


**Figure 1.** Boundary position vs. time. Data points: a - upper image, b - lower image.

Exemplary in Fig. 1, the boundary position is shown vs. annealing time of an individual nearly plane high angle boundary at about 603 K and 25 T in a Zn (99.99+%) bicrystalline sample (2x4x15mm<sup>3</sup>). It shows a constant boundary velocity (0.049x10<sup>-3</sup>m/s) over a macroscopic distance of about 2 mm. The difference in free energy density due to the misalignment of both grains with the field is approximately 1.2 KJ/m<sup>3</sup> (<5141> 81° asymmetric tilt grain boundary). From this the absolute mobility of this boundary structure at this temperature ( $m=v/p$ ) becomes 4.1x10<sup>-8</sup> m<sup>4</sup>/Js.

### Acknowledgements

Financial support from the Deutsche Forschungsgemeinschaft (GO 335/24, MO 848/4) as well as Dr. Scott T. Hannahs' technical support are gratefully acknowledged.

### References

- 1 Mullins, W.W., *Acta Met.*, **4**, 421-432 (1956).
- 2 Molodov, D.A., *et al.*, *Scr. Mat.*, **8**, 1207-1213 (1997).
- 3 Konijnenberg, P.J., *et al.*, *Mat. Sc. For.*, **467-470**, 763-770 (2004).

**The design and construction of superconducting magnets depends very much on the precise knowledge of the electrical and mechanical properties of the conductor to be used. Detailed characterization is needed, especially of the degradation of the current carrying capability at a temperature of 4.2 K in a magnetic field as a function of the applied stress. A unique and very versatile instrument has been developed and constructed at the NHMFL for this type of measurement. Measurements at different Nb<sub>3</sub>Sn wires have been performed and show that these wires can support a strain level of 0.4 %.**

### IN-FIELD $I_c$ of Nb<sub>3</sub>Sn WIRES UNDER STRAIN

U.P. Trociewitz (NHMFL), R.P. Walsh (NHMFL), V.J. Toplosky (NHMFL), J. Miller (NHMFL)

### Introduction

High current carrying capabilities and strain tolerance are important properties to achieve in superconductors to be used



in successful high field magnet applications. To study the various effects of strain on practical Nb<sub>3</sub>Sn conductor and ultimately to characterize conductor that will be used within high-field magnet projects at the NHMFL, a device has been built to measure the critical current of short wire samples at 4.2 K as a function of strain in a large-bore high-field magnet. The device is operated by a stepper-motor and worm gear assembly and is rated for maximum loads up to 2.5 kN. Tensile strains of 1 % can be easily accommodated. The probe is instrumented with vapor-cooled current leads and high temperature superconducting current lead extensions to allow for transport currents up to 1.5 kA. The setup was operated in the NHMFL large bore resistive magnet in fields up to 20 T.

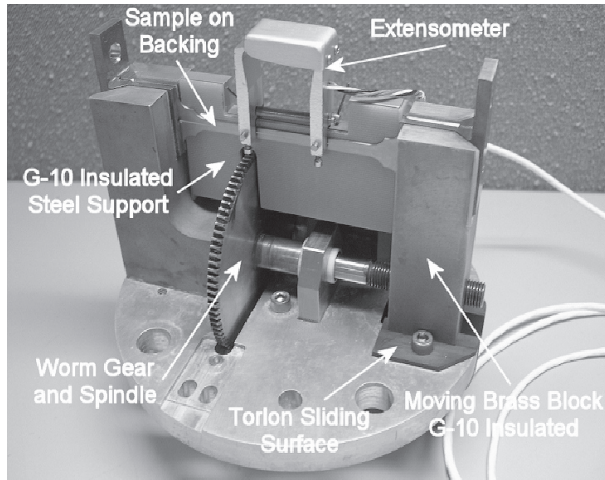


**Figure 1.** View of the strain device. Below the bottom flange (not visible in the picture) is a guiding rod, which is connected to the moving brass block. It moves in a slide bearing that is bolted to the bottom flange and enforces parallel displacement.

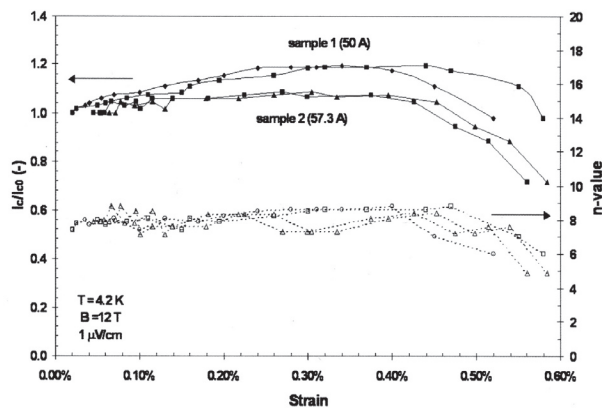


**Figure 2.** top: Normalized  $I_c(\epsilon = 0)$  vs. strain at 4.2 K and 12 T background field for two wire samples of different sections from the same batch. The values in brackets represent the maximum currents achieved under strain. Bottom:  $n$ -values of the samples vs. applied strain.

## Experimental

Fig. 1 shows the complete probe and the strain device. The strain device consists of two brass blocks, between which the sample is mounted. One of the blocks is bolted to the bottom flange and the other can move freely operated by a stainless steel spindle and worm gear assembly, which is driven by a stepper motor on the outside of the cryostat. At a thread pitch of 24 inch<sup>-1</sup> one turn of the stepper motor translates to 0.011 mm linear displacement of the brass block. This ratio provides sufficient resolution for the strain data. In this configuration the whole setup is rated for tensile loads up to 2.5 kN. The setup allows for characterization of short sample lengths of 130 mm.

## Results and Discussion

Preliminary experiments were conducted on research grade Nb<sub>3</sub>Sn wire samples of 0.42 mm diameter.  $I_c$  ratios vs. strain data for two samples from different sections of a wire batch are shown in Fig. 2 (top). Both samples have peak  $I_c$  values of 50 A and 57.3 A at strain values of about 0.30 %, averaged over two strain gauges mounted on each sample. Fig. 2 (bottom) shows the  $n$ -values as a function of the applied strain. Up to about 0.4 % strain, the  $n$ -values for both samples stay almost constant at around  $n = 8$ . Above 0.4 % strain, the  $n$ -values drop to  $n = 5$  indicating the beginning of mechanical damage to the samples. Microstructural analysis on sections of the conductor material revealed irregularities in the filament geometry, which contributed to low  $n$ -values. Further modifications and experiments, allowing the use of an extensometer for the strain characterization, are in progress.

## Reference

- U.P. Trociewitz, *et al.*, submitted to *IEEE Transactions on Applied Superconductivity* (2004).

The report by Canfield *et al.* is an important advance, recently published in *Physical Review Letters*, in our understanding of the role of defects and doping in the  $\text{MgB}_2$  class of materials. Previous work at the NHMFL has shown a dramatic increase in  $H_{c2}$  with carbon doping. The suppression of  $T_c$  with neutron damage and subsequent recovery by annealing show the fundamentally different behavior from the effects of carbon doping. This ability to separate the effects of different induced defects in the material will significantly enhance our understanding of the underlying coupling and isolate the effects of the different scattering channels. In related work by Larbalestier *et al.*, similar carbon-doped  $\text{MgB}_2$  conductor performance was reported using a scalable manufacturing process. The ultimate goal of these investigations could be significantly improved superconducting wires for next-generation superconducting magnets. These reports are prime examples of the NHMFL serving competing groups in a rapidly-developing area of research, in which sample preparation and preliminary measurements are made at other facilities and the NHMFL provides key measurements at the highest obtainable magnetic fields.

## IMPROVED $H_{c2}$ IN BULK-FORM MAGNESIUM DIBORIDE BY MECHANICAL ALLOYING WITH CARBON

B.J. Senkowicz, J.E. Giencke, S. Patnaik, C.B. Eom, E.E. Hellstrom, D.C. Larbalestier (Applied Superconductivity Center, University of Wisconsin)

### Introduction

Recent studies of magnesium diboride thin films by Braccini *et al.*<sup>1</sup> found  $H_{c2}(0K) \parallel > 50$  T for C-doped  $\text{MgB}_2$  films. Such critical field properties exceed those of any Nb-based conductor at any temperature, suggesting that  $\text{MgB}_2$  could be a viable replacement for  $\text{Nb}_3\text{Sn}$  as a high field magnet conductor. Untextured carbon-doped filaments fabricated by a CVD method can achieve upper critical fields in excess of 30 T at 4.2 K<sup>2</sup>.

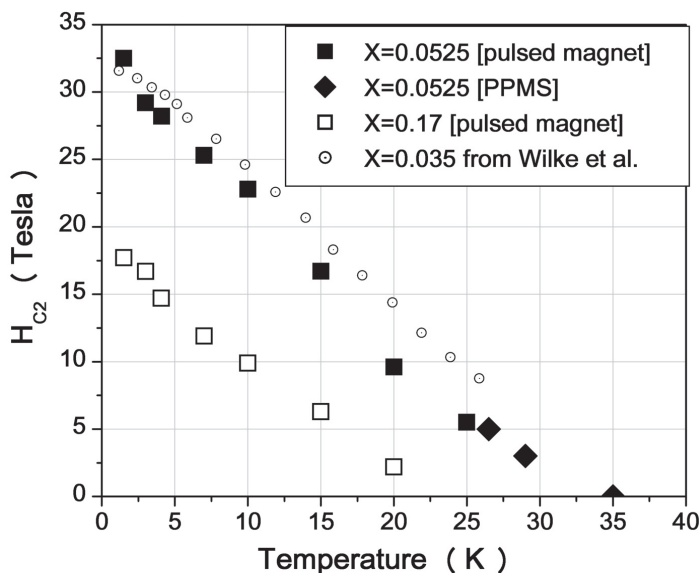


Figure 1.  $H_{c2}$  defined by the 90% normal state resistivity of our carbon-doped samples and final onsets of resistance for the sample of Wilke *et al.*<sup>2</sup>

The present document discusses the *ex-situ* synthesis of alloyed  $\text{MgB}_2$  powder using high energy ball milling of  $\text{MgB}_2$  with C. Since a major goal of  $\text{MgB}_2$  technology is the fabrication of high critical current density, multifilament wire suitable for magnet applications, we need a scalable bulk process capable of producing carbon-doped precursor powder. One such method is provided by this work.

### Experimental

$\text{MgB}_2$  powder was mixed with powdered graphite in several proportions and high energy ball milled for tens of hours, then made into pellets. Pellets were hot isostatic pressed (HIP) at 1000°C and >30 ksi for 200 minutes, then exposed to Mg vapor at 900°C for 5 hours. Properties were then measured by various techniques. High field electrical properties were measured at NHMFL – Los Alamos using the 65 T pulsed magnet.



## Results and Discussion

Figure 1 shows measured  $H_{c2}$  for our samples, plotted alongside data from the literature, where  $x$  is the carbon content given by  $Mg(B_{1-x}C_x)_2$ . Our analyses showed that while our  $X=0.0525$  sample had near total carbon incorporation into the lattice, our nominally  $X=0.17$  sample had a lattice composition of only about  $X=0.69$ . While the  $X=0.0525$  sample had  $J_c > 10^6$  A/cm<sup>2</sup> as well as excellent  $H_{c2}$ , the nominal  $X=0.17$  sample had  $J_c$  reduced by nearly two orders of magnitude. Normal state resistivity was also much higher for the more heavily doped sample.

## Conclusions

We have shown that milling C with  $MgB_2$  can produce  $H_{c2}(0K)$  equal to that obtained for single crystals and CVD filaments. Lattice disorder introduced in the milling process is indicated by weakened XRD patterns and high normal state resistivity. Excess carbon not incorporated into the crystal lattice can result in detrimental effects such as grain boundary obstruction (causing reduced  $J_c$ ), reduced  $T_c$ , and reduced  $H_{c2}$ .

## Acknowledgements

BJS was supported by the Fusion Energy Sciences Fellowship Program, administered by Oak Ridge Institute for Science and Education under a contract between the U.S. Department of Energy and the Oak Ridge Associated Universities. This research was also supported by the NSF under the University of Wisconsin-Madison MRSEC program. The authors thank the excellent staff of the NHMFL-Los Alamos as well as W. Starch, A. Squitieri, J. Mantei, and R. Mungall in Wisconsin.

## References

- <sup>1</sup> V. Braccini *et al.*, *Cond. Mat.* 0402001, (2004). *Phys. Rev. B.*, **71**, 01254 (2005).
- <sup>2</sup> R.H.T. Wilke *et al.*, *Phys. Rev. Lett.*, **92**, 217003-1 (2004).

## EFFECTS OF CARBON DOPING AND NEUTRON IRRADIATION ON THE UPPER CRITICAL FIELD OF $MgB_2$

R. Wilke (ISU, Ames Lab), D. Finnemore (ISU, Ames Lab), S. Bud'ko (Ames Lab), P. Canfield (ISU, Ames Lab), S. Hannahs (NHMFL), R. Suplinskas (Specialty Materials), J. Farmer (MURR)

## Introduction

$MgB_2$ <sup>1</sup> is a conventional phonon mediated BCS superconductor with the unconventional property of having two superconducting gaps.<sup>2</sup> Three scattering rates associated with the two ( $\sigma$  and  $\pi$ ) bands influence the temperature dependence of the upper critical field. Theoretical calculations predict different developments of  $H_{c2}$  if the scattering rates can be selectively tuned.<sup>3</sup> The enhancement of  $H_{c2}$  through carbon doping<sup>4</sup> has been attributed to an increase in scattering in the  $\pi$  band.<sup>5</sup> Neutron damage studies on pure  $MgB_2$  wire segments show a suppression of  $H_{c2}$  that approximately scales with  $T_c$ .<sup>6</sup> We have irradiated  $Mg(B_{.962}C_{.038})_2$  to study the interplay between two different types of defects.

## Experimental

Carbon doped boron filaments were prepared using a chemical vapor deposition system at Specialty Materials. Filaments were converted to  $MgB_2$  by exposure to magnesium vapor at elevated temperatures. These samples were exposed to fluences of  $7 \times 10^{18}$  thermal neutrons at the Missouri University Research Reactor. Upper critical field values were determined using the onset criteria in transport measurements. Resistance vs. temperature was measured in fields up to 14 T in a Quantum Design PPMS at Ames Laboratory and resistance vs. field was measured using a lock in technique in a 32.5 T resistive magnet at the NHMFL in Tallahassee, FL.

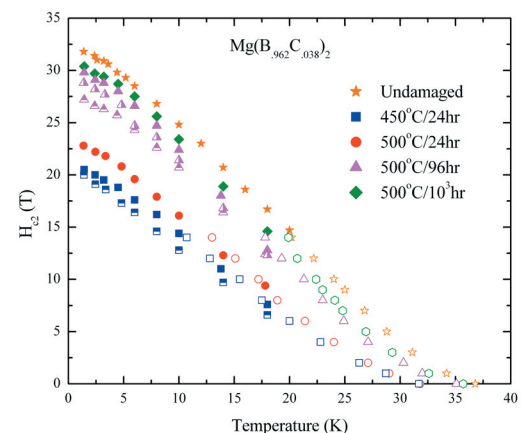
## Results and Discussion

The  $7 \times 10^{18}$  fluence fully suppressed superconductivity in the  $Mg(B_{.962}C_{.038})_2$  samples. Superconductivity was restored by post exposure annealing for various times and temperatures. For example, a 24 hour anneal at 300°C gave  $T_c$  near 20 K. Figure 1 presents  $H_{c2}$  data for samples which had  $T_c > 30$  K.  $H_{c2}(T=0)$  scales with  $T_c$  for each of the irradiated samples. This behavior is analogous to the case of neutron damaging in pure

$MgB_2$  and in contrast to the effects of carbon doping alone. The effects of scattering, resulting from defects introduced by exposure and subsequent annealing, appear to act independently of the effects produced by the presence of carbon.

## Conclusions

The transition temperature for neutron damaged carbon doped  $MgB_2$  filaments was tuned by the post exposure annealing. For the full range of  $T_c$ s accessed by this method,  $H_{c2}(T=0)$  approximately scaled with  $T_c$ , suggesting neutron damage acts to globally suppress superconductivity and doesn't selectively enhance any specific scattering channel.



## Acknowledgements

Ames Laboratory is operated for the U.S. Department of Energy by Iowa State University under Contract No. W-7405-Eng-82. This work was supported by the Director for Energy Research, Office of Basic Energy Sciences.

## References

- <sup>1</sup> Nagmatsu, J., *et al.*, *Nature* (London, United Kingdom), **410**, 6824 (2001).
- <sup>2</sup> Fisher, R.A., *et al.*, *Physica C*, **385**, 180-191(2003).
- <sup>3</sup> Gurevich, A., *Phys. Rev. B*, **67**, 184515 (2003).
- <sup>4</sup> Wilke, R.H.T., *et al.*, *Phys. Rev. Lett.*, **91**, 217003 (2004).
- <sup>5</sup> Angst, M., *et al.*, LANL preprint archive, 0410722 (2004).
- <sup>6</sup> Wilke, R.H.T., *et al.*, unpublished.

**The generation of pulsed high magnetic fields is a major engineering challenge due to the enormous Lorentz forces, which have to be handled reliably. The step from the successful 65 T user magnet to the new 75 T user magnet corresponds to an increase in stress of over 30 %. A series of research reports describes the recent developments at the NHMFL. The efforts not only include a precise failure analysis of one magnet after 470 full field shots, but also material evaluation, in this case a new insulation technique, which must withstand the high compressive forces between the turns and maintain its electrical integrity (see online Swenson, *et al.*, “Evaluation of High Voltage Breakdown Properties of Zylon Served Kapton Insulation System Under Cyclic Compression”). The new poly-layer technique represents a breakthrough in magnet design, which was necessary to pave the road toward 100 T inserts (see online Marshall, *et al.*, “Design Enhancements to the New NHMFL Pulsed Magnets for Improved Performance and Manufacturability”). In “Coil Fabrication Technology Development for Copper Niobium Pulsed Magnet Conductors,” Marshall *et al.* describe design improvements to manufacture repeatable and predictable coil geometries. The efforts have been crowned by the very satisfying performance of the 75 T prototype insert, which not only generated this field reliably, but also offers a longer pulse time and shorter cooling time.**

## INSPECTION OF 65 T PROTOTYPE AFTER LONG TERM OPERATION

C.A. Swenson, W.S. Marshall, E.L. Miller, K.W. Pickard, (NHMFL-FSU)

### Introduction

A prototype 65 T magnet assembly failed after 470 full field science shots. The fault was traced to the inner “A” coil inside the nested two coil assembly. The construction of the inner “A” coil assembly is based upon the poly-layer assembly technique developed for the 100 T insert program. The fault was unique in that the entire magnet assembly was intact save for the winding layer that failed (see Fig. 1). Inspection and analysis of the assembly presented an opportunity to examine all internal interfaces to evaluate structural performance of components after long term service. Such inspection and design review is critical to the practical improvement of pulsed magnets. The inspection of the assembly allows direct evaluation of the structures used in the poly-layer assembly planned for the 100 T insert magnets.

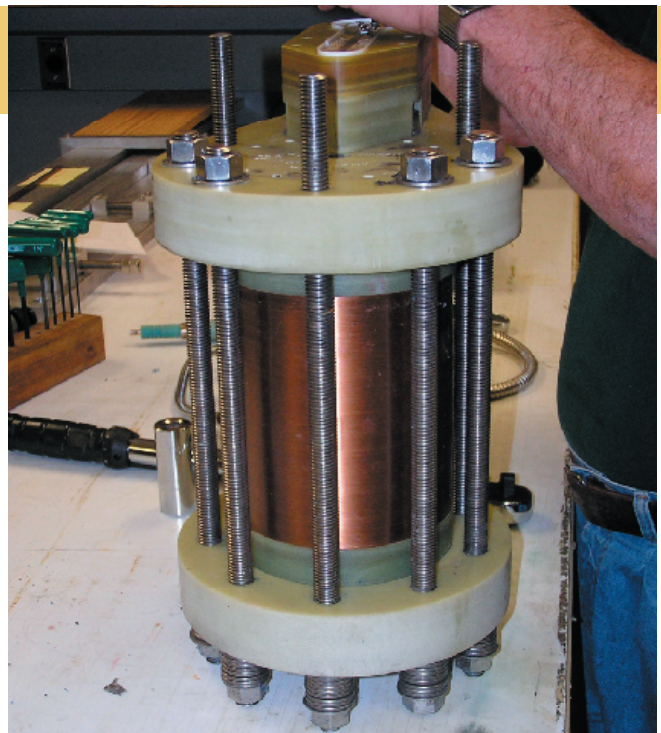


Figure 1. 65 T Assembly at start of inspection.



## Observations

The first operational fault was located in the mid-plane of layer one in the “A” coil insert winding. (See Fig. 2) There is evidence of extreme heat as  $\sim \frac{1}{2}$  of two turns were vaporized. The metal vapor burned through the layer-one zylon reinforcement and MP35N metal reinforcement. Atomized metal particles were observed to be condensed upon the internal radius of the layer two windings. There was no evidence of an electrical fault to layer two.

Electrical insulation structures and lead structures were intact and functioning as designed with no evidence of degradation after long term operation. Geometrical measurements were made on each layer at the winding diameter and the inside diameter of the metal reinforcement. No deformation was observed. Measured dimensions were essentially as constructed.

## Summary

The hypothesis after gross morphological examination is that the kapton™ wire insulation failed via mechanical compression. The two mid-plane turns short circuited initiating an electrical arc. The arc burned insulation and conductor between the turns progressively ablating metal from both wires. The temperature of the shorted turns increased rapidly due to heating from the plasma and the magnet current. It is interesting to note that the axial magnetic field in the mid-plane region will focus a plasma discharge concentrating the heating in one location. The pulsed conductor insulation has since been upgraded to a zylon-kapton system that can take cyclic compression associated with high field operation.

## TRAINING PERFORMANCE OF 75 T PROTOTYPE PULSED MAGNET

C.A. Swenson, W.S. Marshall, E.L. Miller, K.W. Pickard, A. Gavrilin, (NHMFL-FSU);  
D.G. Rickel, J.S. Schilig, (NHMFL: Pulsed Field Facility)

## Introduction

A new 75 T pulsed magnet design is now undergoing operational evaluation at the NHMFL Pulsed Field Science Facility (See Fig. 1). The magnet design incorporates improvements to the engineering template developed for the 65 T pulsed user magnets. The development of the 75 T magnet is part of the NSF effort to develop insert magnets for the DOE 100 T multi-shot (MS) magnet program. An important objective of the 75 T project is to gain experience operating insert-like coils in the same temperature, stress, and strain range encountered at 100 T. The 75 T magnet assembly is comprised of two solenoid coils nested together. The inner “A” coil is constructed with materials and techniques identical to those planned for the 100 T inserts.

The 75 T testing protocol entails three phases of operation: (1) Training and operation at 75 T. (2) Magnet operation at 70 T to baseline reliability performance at 90 T operational stress. (3) Demonstration of cryogen free operation at 70 T. We report the results of phase 1 in this article. This experimental activity is critical for insert design validation.



Figure 2. Layer 1 mid-plane fault illustrating short between turns.

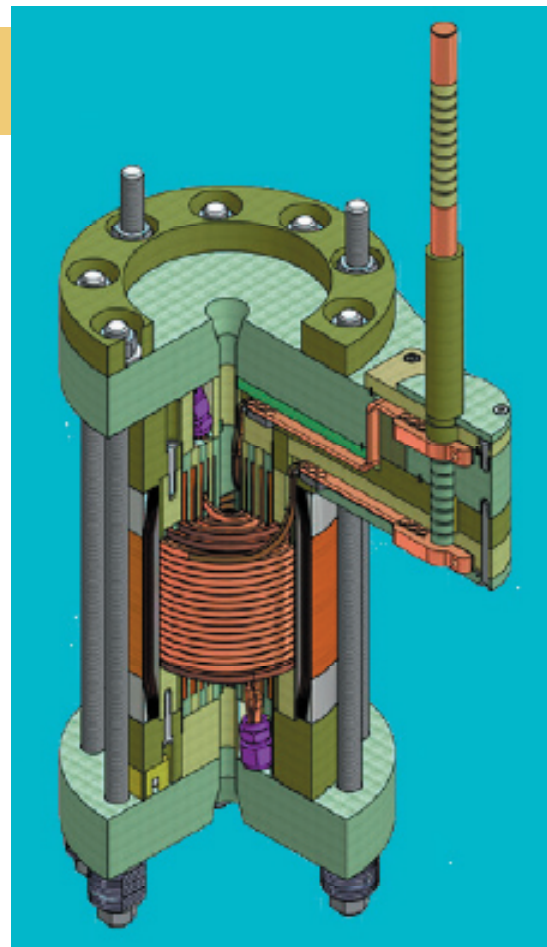


Figure 1. Section view of 75 T with windings.

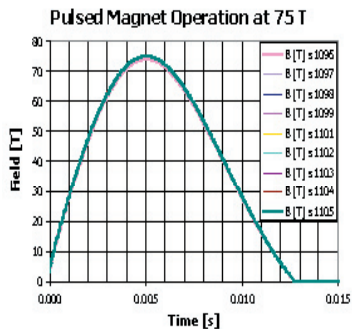


Figure 2. Pulsed field waveforms integrated from B-Dot signal.

## Experimental Results

The 100 T capacitor bank is configured to 15.2 mF for high-energy pulsed operations with the 75 T magnet. We successfully trained the 75 T prototype to full field over 21 pulses of increasing intensity. The capacitor bank energy for a 75 T pulse is 1.44 MJ. We energized the magnet ten times to 75 T in accordance with the test protocol (See Fig. 2). The “100 T Intensity” phase of the testing protocol was completed on November 18. The 75 T testing protocol entails pulses at 70 T to validate reliability at stress levels comparable to the MS Insert at 90 T and cryogen free operation.

## Summary

Magnet performance closely followed design predictions. The drive voltage calculation was within 50 volts of the measured experimental value. The 75 T prototype and the insert capacitor bank both operated together according to specification. The 100 T insert capacitor bank functioned flawlessly throughout training. We are optimistic and encouraged by the technical results obtained thus far.

# CONDENSED MATTER PHYSICS

**S**ingle-walled carbon nanotubes (SWNTs), tubular crystals of  $sp^2$ -bonded carbon atoms that are just one atom thick, come in different varieties, each with a subtle difference in structure and properties – some of them are metals and others are semiconductors. However, their basic electronic properties can change when they are placed inside a magnetic field. Specifically, the band gap is predicted to oscillate with period  $\phi_0 = h/e$ , (i.e., the magnetic flux quantum), and thus, metallic tubes become semiconducting even in an infinitesimally small magnetic field and semiconducting tubes can become metallic in ultrahigh magnetic fields<sup>1</sup>. Furthermore, the Kramers degeneracy between the K and K' points can be lifted by a magnetic field. See Fig. 1. Consequences of these band structure changes are expected to appear in interband optical spectra as peak shifts and splittings. Here, we performed the first magneto-optical study on SWNTs in DC magnetic fields up to 45 T, verifying some of the predictions<sup>2</sup>. We clearly observed that the band gaps of semiconducting SWNTs shrink steadily with magnetic field. We also observed significant field-induced optical anisotropy as well as splittings of absorption and photoluminescence peaks, quantitatively consistent with the predictions. This behavior is unique among known materials, and it is a direct consequence of the change in the circumferential boundary condition through the Aharonov-Bohm phase. The Aharonov-Bohm effect has been observed in other physical systems, but this is the first case where the effect interferes with another fundamental solid-state theorem, that is, the Bloch theorem. We are already extending this exciting work to higher magnetic fields, using the pulsed field facilities in Toulouse, Los Alamos, and Berlin. In even higher magnetic fields ( $\sim 2000$  T), we expect the gap to disappear altogether, causing the semiconducting nanotubes to transform into metals.

## INTERBAND MAGNETO-OPTICAL STUDIES OF SINGLE-WALLED CARBON NANOTUBES IN HIGH DC MAGNETIC FIELDS UP TO 45 T

S. Zaric, G.N. Ostojic, J. Kono (Rice U., ECE); J. Shaver, V.C. Moore, R.H. Hauge, R.E. Smalley (Rice U., Chemistry); X. Wei (NHMFL, Tallahassee)

### Introduction

The band structure of a single-walled carbon nanotube (SWNT) is predicted to depend on the Aharonov-Bohm (AB) phase  $2\pi\phi/\phi_0$  ( $\phi_0$ : magnetic flux quantum). Consequences are expected to appear in

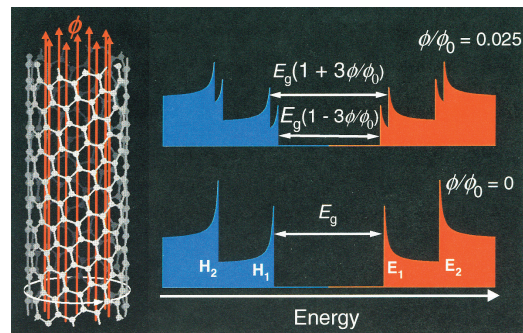
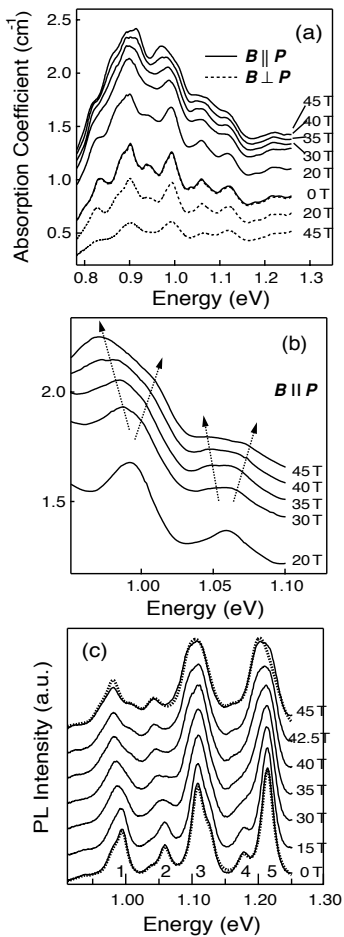


Figure 1. Schematic diagram showing band structure modifications induced by a magnetic flux threading a single-walled carbon nanotube.





**Figure 2.** (a) Polarization-dependent absorption spectra. Solid (dashed) lines are for parallel (perpendicular) polarization. No traces are offset. (b) Expanded plot for the  $B||P$  case from 20 T to 45 T. (c) PL spectra. Solid (dashed) lines correspond to measured (fitted) data. The chiralities of the dominant peaks are 1: (10,3), 2: (8,6), 3: (7,6), 4: (10,2), 5: (7,5).

interband optical spectra as peak shifts and splittings. Here we report the first magneto-optical study on SWNTs, revealing the predicted peaks shifts and splittings.<sup>2</sup>

### Experimental

The nanotube solution was contained in a quartz cell, mounted with a polarizer on a specially designed sample stick with integrated optic fibers, lenses, and mirrors. All measurements were done at room temperature.

## Results and Discussion

Figure 2(a) shows polarization-dependent absorption in the Voigt geometry. The solid (dashed) lines are for parallel (perpendicular) polarization. The field induces optical anisotropy. Also, each peak broadens with  $B$  [Fig. 2(b)]. Figure 2(c) shows PL spectra up to 45 T. All peaks shift to lower energy, and the shift is more obvious for lower energy peaks.

These data can be explained in terms of the AB-effect-induced splitting and magnetic alignment of tubes. The obtained values for 45 T splitting are comparable to the predicted values, and an order of magnitude larger than the Zeeman splitting.

### Conclusions

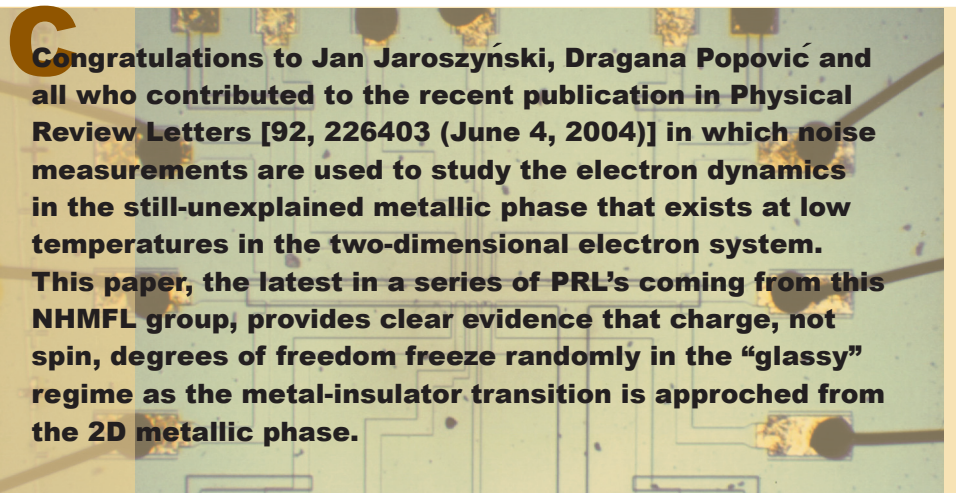
We have performed magneto-optical experiments on SWNTs up to 45 T, confirming theoretical predictions that the band structure of a SWNT is dependent on the magnetic flux,  $\phi$ , threading the tube.

### Acknowledgements

This work was supported by the Robert A. Welch Foundation (No. C-1509), the Texas Advanced Technology Program (No. 003604-0001-2001), and the National Science Foundation (No. DMR-0134058).

### References

- 1 Ajiki, H. and Ando, T., *J. Phys. Soc. Jpn.* **62**, 1255 (1993).
- 2 Zaric, S., *et al.*, *Science*, **304**, 1129-1131 (2004); *Nano Lett.*, **4**, 2219-2221 (2004).



**Congratulations to Jan Jaroszyński, Dragana Popović and all who contributed to the recent publication in Physical Review Letters [92, 226403 (June 4, 2004)] in which noise measurements are used to study the electron dynamics in the still-unexplained metallic phase that exists at low temperatures in the two-dimensional electron system. This paper, the latest in a series of PRL's coming from this NHMFL group, provides clear evidence that charge, not spin, degrees of freedom freeze randomly in the "glassy" regime as the metal-insulator transition is approached from the 2D metallic phase.**

## TIME-DEPENDENT CONDUCTANCE FLUCTUATIONS IN THE METALLIC PHASE OF A TWO-DIMENSIONAL ELECTRON SYSTEM IN SILICON

J. Jaroszyński, D. Popović (NHMFL); T.M. Klapwijk (Delft Univ. of Technology, Applied Physics)

### Introduction

The interplay between strong Coulomb interactions and disorder is believed to be responsible for many surprising and intriguing experimental observations that suggest the existence of a metallic phase in two dimensions (2D).<sup>1</sup> One of the central unresolved issues involves the role of the electrons' spins. Our studies of low-frequency resistance noise<sup>2,3</sup> in a 2D electron system (2DES) in Si have revealed a dramatic change in the electron dynamics that occurs near the metal-insulator transition (MIT) as it is approached from the metallic side. This change in the dynamics, attributed to glassy freezing, persists even when the electrons are fully spin polarized indicating that charge, not spin, degrees of freedom are responsible for

glassy ordering. On the other hand, the origin of the  $1/f$  resistance noise observed in the metallic phase has not been understood. In disordered metals at low temperatures, slow atomic motion gives rise to  $1/f$  noise via the mechanism of universal conductance fluctuations (UCF).<sup>4</sup> Such noise is suppressed by a magnetic field  $B$  in a very specific way.<sup>5</sup> In order to shed light on the origin of noise in the metallic phase, we have studied the effect of a parallel  $B$  on noise, and compared our results to theoretical predictions.<sup>5</sup>

## Experimental

Measurements of resistance as a function of time for a fixed carrier density  $n_s$  and in fixed parallel  $B$  of up to 9 T were carried out on a high-mobility ( $\mu \approx 2.5 \text{ m}^2/\text{Vs}$  at 4.2 K) 2DES in Si using a standard four-probe lock-in technique at 2.7 Hz. The samples and the measurement technique have been described in more detail elsewhere.<sup>3</sup>

## Results and Discussion

The noise power for  $n_s$  in the metallic phase is suppressed by a parallel  $B$ , and the spectrum changes from  $1/f$  to  $1/f^{0.5}$ . This suppression of noise suggests that its origin is probably related to the electrons' spins. In case of UCFs, the theory predicts<sup>5</sup> that the variance of conductance,  $(\delta G)^2$ , will be reduced exactly by a factor of 2 in a parallel  $B$  because of the Zeeman splitting, but it does not predict any change in the power spectrum. Fig. 1 shows that, in our samples,  $(\delta G)^2$  is reduced by almost two orders of magnitude before it becomes more or less independent of  $B$  for  $B > 4$  T, where the 2DES is spin polarized.

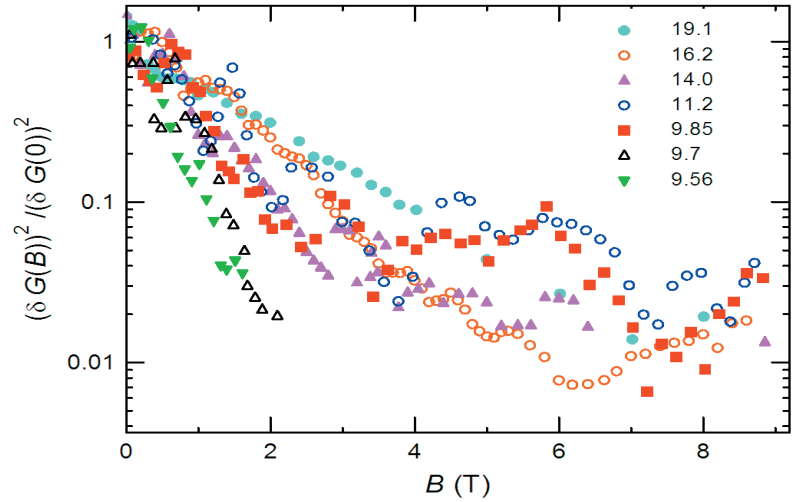


**Figure 1.** The  $B$ -field dependence of the conductance fluctuations for several densities  $n_s$  ( $10^{10} \text{cm}^{-2}$ ) from 9.56 to 19.1 at  $T=0.24$  K.

## Conclusions

We have established that the  $1/f$  resistance noise observed in the metallic regime of a 2DES in Si does not result from the motion of impurities and UCFs, but rather it appears to originate from some type of spin scattering. One possibility includes disorder-induced local magnetic moments, but a detailed mechanism presents yet another puzzle in the understanding of this novel metallic phase.

## Acknowledgements

This work was supported by NSF Grant No. DMR-0071668 and the NHMFL. We are grateful to V. Dobrosavljević for useful discussions.

## References

- <sup>1</sup> Abrahams, E., *et al.*, *Rev. Mod. Phys.*, **73**, 251 (2000); Kravchenko, S.V. and Sarachik, M.P., *Rep. Prog. Phys.*, **67**, 1 (2004), and references therein.
- <sup>2</sup> Bogdanovich, S. and Popović, D., *Phys. Rev. Lett.*, **88**, 236401 (2002).
- <sup>3</sup> Jaroszyński, J., *et al.*, *Phys. Rev. Lett.*, **89**, 276401 (2002); Jaroszyński, J., *et al.*, *Phys. Rev. Lett.*, **92**, 226403 (2004).
- <sup>4</sup> Feng, S., *et al.*, *Phys. Rev. Lett.*, **56**, 1960 (1986).
- <sup>5</sup> Stone, A.D., *Phys. Rev. B*, **39**, 10736 (1989).



**C**ongratulations to Scott Crooker, Dwight Rickel, and colleagues for their article “Spectroscopy of spontaneous spin noise as a probe of spin dynamics and magnetic resonance” that appears in the September 2 issue of *Nature* magazine and establishes the usefulness of noise spectroscopy as a perturbation-free probe of spin dynamics and magnetic resonance. As devices shrink in size to the nanoscale regime, fewer atoms and spins dominate the device behavior and noise fluctuations become more prominent. By drawing on the fluctuation-dissipation theorem, this work, to appear in the next issue of *NHMFL Reports*, firmly establishes that one scientist’s noise is another scientist’s signal. Conventional magnetic resonance techniques, such as those used in magnetic resonance imaging (MRI) machines, require the excitation and absorption of specific radio-frequency waves by atoms in a magnetic field. These absorption patterns can be used to reveal molecular and magnetic properties . . . and even make a medically useful image. Instead of “shining” radio-frequency waves on the sample, the NHMFL researchers simply “listen” very carefully to the tiny, intrinsic thermal and quantum-mechanical fluctuations of a group of magnetic spins—called spin noise. They demonstrate that those fluctuations are able to reveal a number of the same properties without having to disturb it from its natural resting state. Using a laser technique known as Faraday rotation, the scientists measured the spectrum of spin noise in vapors of magnetic rubidium and potassium atoms. The noise spectrum alone revealed the complete magnetic structure of the atoms. This research might pave the way for magnetic resonance imaging techniques that are useful in fields like nanotechnology and quantum information science where systems containing only a few atoms are becoming commonplace and their associated magnetic fluctuations play an increasingly dominant role.

## MEASURING RANDOM SPIN FLUCTUATIONS FOR PERTURBATION-FREE PROBES OF SPIN DYNAMICS AND MAGNETIC RESONANCE

S.A. Crooker, D.G. Rickel (NHMFL-LANL); A.V. Balatsky, D.L. Smith (Theory Division, LANL)

### Introduction

In magnetic systems, fundamental noise can exist in the form of random spin fluctuations. In his seminal 1946 paper on nuclear induction, Felix Bloch noted that random, statistical fluctuations of  $N$  paramagnetic spins should generate measurable noise of order  $N^{1/2}$  spins, even in zero magnetic field. By the fluctuation-dissipation theorem, this “spin noise” alone contains detailed information about the spin system itself. (The fluctuation-dissipation theorem states that the response of a system to an external perturbation— *i.e.*, the susceptibility—can be described by its spectrum of fluctuations while in thermal equilibrium). We are using optical techniques to passively and sensitively “listen” to the magnetization noise in a classical, equilibrium ensemble of paramagnetic alkali atoms.<sup>1</sup> Correlation spectra of the measured spin noise reveals the complete magnetic structure of the atomic  $^2S_{1/2}$  ground state ( $g$ -factors, nuclear spin, isotope abundance ratios, hyperfine splittings, nuclear moments, and spin coherence lifetimes)—without having to excite, optically pump, or otherwise drive the system away from thermal equilibrium.

### Results and Discussion

A linearly polarized laser, detuned from any atomic absorption, is focused through a cell containing rubidium or potassium vapor (Fig. 1a). Random magnetization fluctuations along  $z$  impart small polarization (Faraday) rotation fluctuations  $\delta\theta_r(t)$  on the laser, which are sensitively measured with a balanced photodiode bridge. Helmholtz coils provide a small transverse magnetic field  $B$  along  $x$ , about which all magnetization fluctuations  $\delta M_z$  must precess. The detuned laser ensures that atoms are not optically pumped or excited in any way. The spin correlation function,  $S(t) = \langle M_z(0)M_z(t) \rangle$ , has a Fourier transform  $S(\omega)$  that is related simply to the power spectrum of  $\delta\theta_r(t)$ . A typical noise spectrum is shown in Fig. 1b. The sharp peaks at  $\Omega = 869$  and  $1303$  kHz are due to random spin fluctuations which are precessing

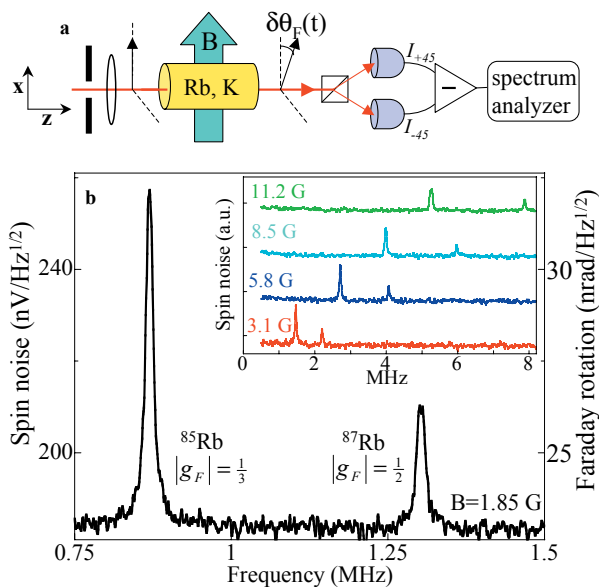


**Figure 1.** (a) Experimental schematic. (b) Spin noise spectrum in Rb vapor at 369 K and 1.85 G, showing spontaneous spin coherence peaks from  $^{85}\text{Rb}$  and  $^{87}\text{Rb}$ . Inset: Noise peaks vs. magnetic field (offset vertically for clarity).

in the small 1.85 G transverse magnetic field, effectively generating spontaneous spin coherences between ground-state Zeeman sublevels. These coherences precess with  $g$ -factors  $\sim 1/3$  and  $1/2$ , which are the ground-state  $g$ -factors of the stable isotopes  $^{85}\text{Rb}$  and  $^{87}\text{Rb}$ . Coupling of the nuclear spin  $I$  to the  $J=1/2$  valence electron splits the  $^2S_{1/2}$  atomic ground state into two hyperfine levels with total spin  $F = I \pm J$  and  $g$ -factor  $|g_F| \approx g_J / (2I+1)$ , where  $g_J \approx 2$  is the free electron  $g$ -factor. Thus, the nuclear spin of  $^{85}\text{Rb}$  ( $I=5/2$ ) and  $^{87}\text{Rb}$  ( $I=3/2$ ) may be directly measured from spin fluctuations in thermal equilibrium. Strikingly, the measured spin noise actually *increases* when the diameter of the probe laser *shrinks* (Fig. 2). This result may be understood by considering that the Faraday rotation imposed on light passing through an intentionally-magnetized system is independent of beam area, so that the effective measurement sensitivity (rotation angle per unit polarized spin,  $\theta_F/N$ ) is larger for narrower beams. Therefore, fluctuations of order  $N^{1/2}$  spins induce correspondingly more signal. These data suggest the utility of noise spectroscopy for passive probes of small systems, where the absolute amplitude of measured fluctuations actually increases when probe size is reduced, as long as measurement sensitivity increases correspondingly.

## References

- 1 S.A. Crooker, *et al.*, *Nature*, **431**, 49 (2004).

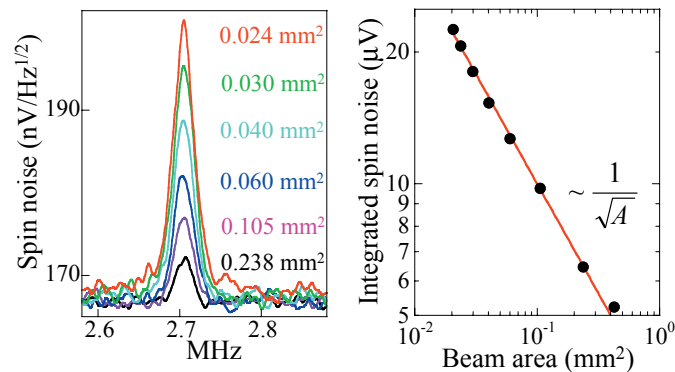


**Figure 2.** Increasing absolute spin noise with decreasing cross-sectional beam area.  $B=5.8$  G, fixed spin density, and constant laser power.

**With a Neel temperature of 10 K,  $\text{CeIn}_3$  is an antiferromagnetic heavy fermion compound situated at the very heart of the debate as to the role of spin fluctuations in unconventional superconductivity. It is of particular interest to quantum criticality theorists owing to its unique simple cubic crystal structure. Superconductivity occurs under pressure at close proximity to a putative pressure-induced quantum critical point at 25 kbar, whereupon the Neel order vanishes. It was recently shown in Los Alamos that the Neel temperature can also be suppressed to zero by applying very big magnetic fields of order 60 T. The present report concerns measurements of the specific heat and magnetocaloric effect that provides unambiguous evidence for the effect of a magnetic field on the Neel ordering temperature.**



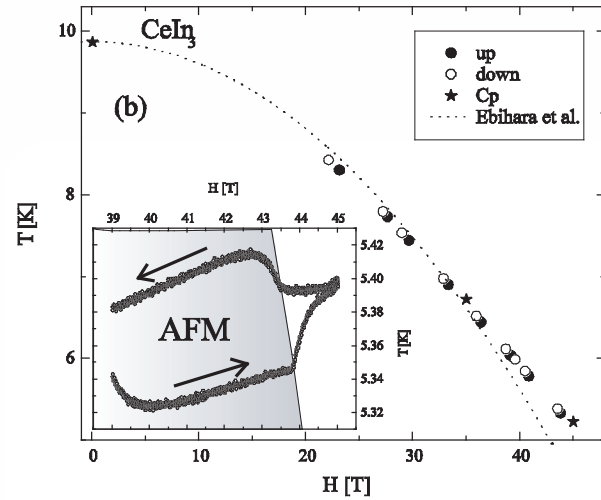
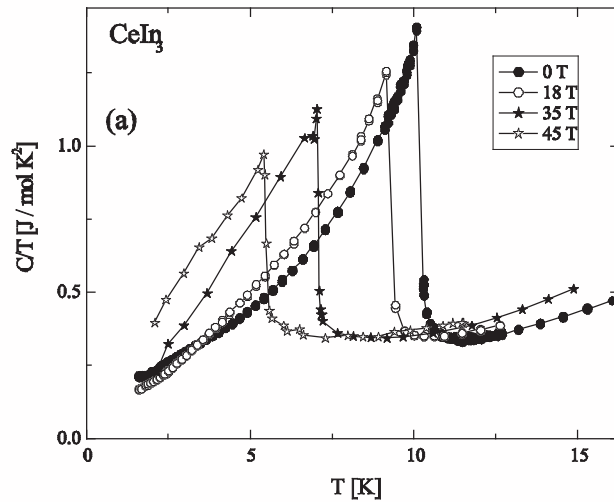


**Figure 1.** (a) Specific heat  $C/T$  as a function of temperature for  $H = 0, 18, 35,$  and  $45$  T. (b) Main Panel: phase boundary determined by specific heat measurements (star symbols) and magnetocaloric effect measurements increasing (solid symbols) and decreasing (open symbols) field. Inset: quasi-adiabatic change of temperature  $T(H)$  during a fast change of magnetic field (MCE).

## HIGH FIELD PHASE DIAGRAM OF CUBIC $\text{CeIn}_3$

A.V. Silhanek; M. Jaime; N. Harrison (MST-NHMFL, LANL); and T. Ebihara (Dep. of Phys., Shizuoka University, Shizuoka 422-8529, Japan)

The  $\text{CeIn}_3$  compound is an intermetallic heavy fermion with a ground state resulting from the competition of a long ranged magnetically ordered state produced by RKKY interactions and the Kondo effect. The former dominates at low temperatures leading to an antiferromagnetic phase (AFM) for temperatures  $T < 10$  K. Under relative small pressure ( $\sim 25$  kbar), however, the screening of the 4f moments by the conduction electrons compensates the RKKY interaction and a particular situation where neither one of the ground state dominates leads to the formation of a quantum critical point (QCP). In a similar fashion the magnetic ordering temperature  $T_N$  may also be suppressed by applying high magnetic fields  $H \sim 60$  T with a possible emerging quantum critical point.

In this work we have determined the  $H$ - $T$  phase boundary of the AFM phase using specific heat (see Fig.1(a)) and magnetocaloric effect (see inset of Fig.1(b)) measurements. The main panel of Fig. 1(b) summarizes the

obtained diagram with star symbols indicating the specific heat measurements and circles symbols corresponding to magnetocaloric effect (MCE) measurements. In the MCE experiments the temperature of the sample is recorded during a rapid sweep of the magnetic field as shown in the inset of Fig. 1(a). Here the phase transition manifests itself as a kink in the quasi-adiabatic  $T(H)$  evolution without any evidence of field irreversibility in agreement with a second order transition.

The phase diagram depicted in Fig. 1(b) exhibits a quadratic field dependence at low fields that turns into a linear dependence at high fields and extrapolates to  $T_N = 0$  at  $H \sim 80$  T. This value is significantly higher than the previous estimations using a quadratic fitting. In any case, these data confirm that as  $T_N \rightarrow 0$ , the slope of the phase diagram remains finite implying that the transition at  $T_N = 0$  is still second order making it a good candidate for quantum criticality.<sup>1</sup>

## References

- <sup>1</sup> Ebihara, T., *et al.*, *Phys. Rev. Lett.*, **93**, 246401 (2004).

**The contributions to the research category “Kondo/Heavy Fermion Systems” were generally of outstanding quality this year, both by the volume and detail of the reported research efforts, as well as by their first-rate scientific content. Most activities concentrated on the central open question in this field—that of the physics of quantum phase transitions. Because of the high quality of the contributions it proved very difficult to select one or two that deserve special attention. This work, however, caught special attention; it reports striking evidence of quantum critical behavior, induced by suppressing antiferromagnetic ordering through the application of high magnetic fields. Both the resistivity and the specific heat data clearly show how the conventional Fermi liquid behavior is suppressed precisely where magnetic ordering is destroyed. Even more interestingly, this work reports the emergence of a novel high-field metallic phase characterized by an unusual T<sup>3</sup> form for the resistivity, in striking contrast to the conventional T<sup>2</sup> behavior found below the critical point. These data thus seem to identify a novel type of quantum critical point, one separating a conventional Fermi liquid from an exotic high-field phase. This work is a perfect example of how the cutting edge experimental tools available at the Magnet Lab continue to uncover tremendously exciting and unexpected phenomena, which will guarantee that our efforts will continue to bloom for many years to come.**

## MAGNETIC FIELD-TUNED QUANTUM CRITICAL POINT IN CeAuSb<sub>2</sub>

L. Balicas (NHMFL); S. Nakatsuji (U. Kyoto, Physics); H. Lee (UC Davis, Physics); P. Schlottmann (FSU, Physics); T. P. Murphy (NHMFL); Z. Fisk (UC Davis, Physics)

### Introduction

When the long-range order in a system is suppressed to zero temperature by tuning an external variable, such as pressure, chemical composition or magnetic field  $H$ , the system is said to exhibit a quantum critical point (QCP).<sup>1</sup> The magnetic field is an ideal control parameter, since it can be reversibly and continuously tuned towards the QCP. Two compounds with field-tuned QCP, YbRh<sub>2</sub>Si<sub>2</sub> and Sr<sub>3</sub>Ru<sub>2</sub>O<sub>7</sub>, reached prominence due to the non-Fermi liquid (NFL) behavior triggered by the quantum fluctuations associated with the QCP. In this report we present a Ce-compound, CeAuSb<sub>2</sub>, exhibiting a field-tuned QCP and unusual transport and thermodynamic properties. All three systems have a field-tuned QCP as a common thread, yet their behavior in high fields and low  $T$  are considerably different.

### Experimental

Here we report on the anomalous metallic properties of CeAuSb<sub>2</sub> having used a combination of cryogenic and high field facilities provided by the NHMFL.

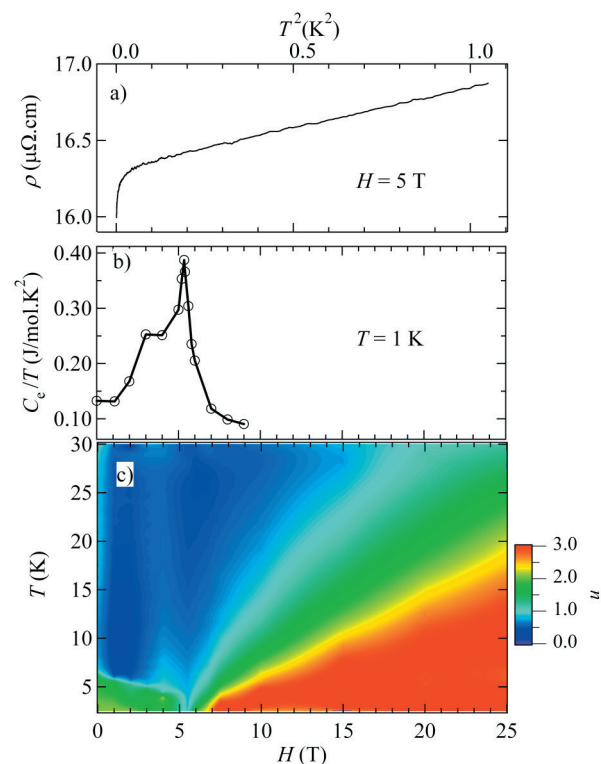


**Figure 1.** a) The  $T^2$ -dependence of  $\rho$  down to  $T \cong 25\text{ mK}$  for  $H = 5\text{ T} \leq H_C$ . Notice the pronounced deviation from the  $T^2$  dependence at the lowest  $T$ , which is observed only in the vicinity of the critical field  $H_C$ . b) The electronic heat capacity as a function of field  $H$  and at  $T = 1\text{ K}$ . c) The exponent  $n$  of the resistivity  $\rho$  in the  $T - H$  plane.



## Results and Discussion

$H = 0$ ,  $\text{CeAuSb}_2$  displays AF ordering at  $T_N = 6.0$  K. Above  $T_N$ , the resistivity  $\rho$  displays a  $T^\alpha$  dependence with  $\alpha < 1$  and  $C_\rho/T$  has the  $-\ln T$  dependence characteristic of NFL behavior. For  $T < T_N$ ,  $\rho$  has the  $AT^2$  FL-like dependence and the extrapolation of  $C_\rho/T$  to  $T = 0$  yields a Sommerfeld coefficient of  $\gamma \sim 0.1$  J/mol.K<sup>2</sup>, so that  $\text{CeAuSb}_2$  is to be considered a heavy-Fermion system. A magnetic field along the inter-plane direction leads to two subsequent metamagnetic transitions and the concomitant *continuous* suppression of  $T_N$  to  $T = 0$  at  $H_C = 5.3 \pm 0.2$  T. As the AF phase boundary is approached from the paramagnetic (PM) phase,  $\gamma$  is enhanced and the  $A$  coefficient of the resistivity diverges as  $H - H_C^{-1}$ . As  $T$  is lowered for  $H \sim H_C$ , the  $T$ -dependence of  $\rho$  and  $C_\rho/T$  is sub-linear and  $-\ln T$ , respectively. These observations suggest the existence of a field-induced QCP at  $H_C$ . At higher fields an unconventional  $T^3$ -dependence emerges and becomes more prominent as  $H$  increases, suggesting that the FL state is *not* recovered for  $H \gg H_C$ .

## Conclusions

The field-tuned QCP systems represent a challenge from the theoretical perspective, since the different compounds have some common aspects, but do *not* seem to belong to the same universality class.

## Acknowledgements

This work is sponsored by the National Nuclear Security Administration under the Stewardship Science Academic Alliances program through DOE grant DE-FG03-03NA00066.

## References

<sup>1</sup> See, for instance, S. Sachdev, *Quantum Phase Transitions* (Cambridge Univ. Press, Cambridge, 1999); For a review in materials and properties see, G.R Stewart, *Rev. Mod. Phys.*, **73**, 797 (2001).

**The conventional view is that the pseudogap in cuprate superconductors arises from phase fluctuations of the energy gap. Gor'kov and Teitel'baum have investigated an alternative point of view, namely the tendency of HTS materials to phase separate. They have shown that the NMR pseudogap behavior can arise from fluctuating aggregates of holes. While at high T the holes form a continuous phase, at a critical temperature  $T^*$  and a first order transition takes place, with strong fluctuations in the size and location of domains occurring. An analysis of the data shown that the  $1/^{63}\text{T}_1$  curves collapse onto a single curve. The domains may be pinned by structural defects. The theory agrees well with data from LSCO.**

## PSEUDOGAP REGIME IN HIGH $T_c$ -CUPRATES AS A MANIFESTATION OF A DYNAMICAL PHASE SEPARATION

L.P.Gor'kov (NHMFL); G.B.Teitel'baum (Zavoiskii Inst., Kazan, Russia)

## Introduction

The popular view is that the pseudogap state in cuprates arises as a crossover in the density of states. We investigated an alternative view taking into account an inherent tendency of high- $T_c$  materials to the phase separation<sup>1</sup> now confirmed by numerous experimental data. Analyzing existing NMR data we have shown<sup>2</sup> that the pseudogap behavior of the nuclear spin relaxation for cuprates may be considered as a manifestation of the frustrated phase separation to the “metallic” (holes enriched) and “AF” (holes depleted) regions. The temperature variation of the relative volumes of the coexisting phases having different fluctuation rates would result in the transfer of the fluctuation spectral weight away from the NMR resonance frequency to be seen as a pseudogap suppression of the relaxation rate.

While at high enough temperatures, itinerant holes and  $\text{Cu } d^9$  spins form a homogeneous phase, at a certain temperature  $T^*(x)$  the first order transition takes place and the frustrated phase separation to the  $x=0$  and to the finite  $x$  phases starts. (For interacting holes rigidly localized on Cu's in the  $\text{CuO}_2$  plane the lattice “liquid-gas” transition at some  $T^*$  is known from the exact solution of the 2D Ising-problem). Taking hole-doped  $\text{La}_{1-x}\text{Sr}_x\text{CuO}_4$ , for the sake of argument, missing (with respect to the Sr ionicity) hole's density in the AF area must be recompensed by local metallic inclusions or droplets with higher hole's content. Tiny structure of sub-phases caused by charge neutrality condition leads to strong fluctuations in island's sizes and positions.<sup>1</sup> Phase boundaries move rapidly, inducing the strong hyperfine field fluctuations (note that a Cu-site merely loses spin when a “metallic” region crosses over the position of that  $^{63}\text{Cu}$  nuclear spin). Experimentally one sees only one nuclear resonance frequency, this provides an evidence in favor of the dynamical picture. We discuss only  $1/^{63}\text{T}_1$  behavior because for cuprates spin fluctuations on Cu-site prevail over the Korringa mechanisms.

## Results and discussion

After the careful analysis of the existing experimental data for the nuclear spin relaxation in different materials, we have found that after an appropriate vertical offset all  $1/^{63}\text{T}_1$  curves collapse onto the same  $T$  dependence above their  $T_c$  and below 300 K.<sup>2,3</sup> In this temperature region the nuclear spin relaxation is a sum from two parallel processes:  $1/^{63}\text{T}_1 = 1/^{63}\text{T}_1(x) + 1/^{63}\text{T}_1(T)$ . Here

$1/^{63}\overline{T}_1(x) > 0$  depends only on temperature and degree of disorder, while  $1/^{63}\overline{T}_1(T)$  depends only on temperature and is very near to the  $1/^{63}\overline{T}_1$  dependence for the two chain's material YBCO 124 above its  $T_c=62$  K. Since for all materials with non-zero  $1/^{63}\overline{T}_1(x)$  incommensurate (IC) magnetic peaks at  $[\pi(1\pm\delta), \pi]$  and  $[\pi, \pi(1\pm\delta)]$  were observed at neutron scattering, we conjectured  $1/^{63}\overline{T}_1(x)$  be related with these IC peaks ( $\delta$  is the IC splitting parameter). For  $\text{La}_{1.86}\text{Sr}_{0.14}\text{CuO}_4$  the detailed experimental data available<sup>4</sup> that provide the correct estimate for the offset  $1/^{63}\overline{T}_1(x)$ .

As for  $1/^{63}\overline{T}_1(T)$ , we ascribe its temperature dependence to the crossover from the *local* regime to the *dynamical* one, when the hyperfine field fluctuates due to the fast variations in the configuration of the  $d^9$  holes surrounding the copper nuclei. In the first case the relaxation is determined by the spin susceptibility, and in the second one by the probability to have the AF hyperfine field at the given nuclei.

To summarize, the nuclear spin relaxation for a broad class of cuprates is due to two independent mechanisms: relaxation on the "stripe"-like excitations and a "universal" temperature dependent term. IC "stripes" always come about with external doping and may be pinned by structural defects. The whole pattern fits well the notion of the dynamical phase separation into coexisting metallic

and IC magnetic phases. Among the most recent of our results is the reconstruction of the 1<sup>st</sup> order phase transition line,  $T^*(x)$ , that agrees well with the phase diagram for LSCO in the (x,T)-plane measured by other means.

## Acknowledgements

The work was supported by the NHMFL through the NSF cooperative agreement No.DMR-0084173 and the State of Florida.

## References

- 1 Gor'kov, L.P., *et al.*, *JETP Lett.*, **46**, 420-425 (1987).
- 2 Gor'kov, L.P., *et al.*, *2003 NHMFL Annual Report*, 317-318 (2004).
- 3 Gor'kov, L.P., *et al.*, *JETP Lett.*, **80**, 195-199 (2004).
- 4 Aeppli, H., *et al.*, *Science*, **278**, 1432 (1997).

**Another very interesting report concerns the T-P phase diagram and magnetoresistance of  $\beta\text{-(BDA-TTP)}_2\text{MBr}_4$  ( $M=\text{Fe, Ga}$ ). In some such materials, the existence of local magnetic moments on ions leads to dramatic changes of the ground state. In other cases, magneto-transport experiments show behavior between magnetic and non magnetic-like. The  $\pi\text{-}d$  interaction is attributed to as the source of this behavior. To understand this  $\pi\text{-}d$  interaction, the T-P phase diagram and the magnetoresistance were thoroughly studied. As  $T$  is decreased, this material undergoes a metal-insulator transition with superconductivity appearing at 12.8 kbar and  $T_c=0.5$  K.**

## INVESTIGATION OF TEMPERATURE-PRESSURE PHASE DIAGRAM AND MAGNETORESISTANCE OF $\beta\text{-(BDA-TTP)}_2\text{MBr}_4$ ( $M=\text{Fe, Ga}$ )

E.S. Choi, J.S. Brooks, S.W. Tozer (Florida State University/NHMFL); J. Yamada (Himeji Institute of Technology, Japan)

The existence of local magnetic moments as magnetic anions in charge transfer salts induces dramatic changes in the ground state of some organic conductors. In other cases, the magnetotransport properties show distinct behaviors between magnetic and non-magnetic compounds even when they show similar ground states. The  $\pi\text{-}d$  interaction was attributed to account for those behaviors, and the magnitude of the interaction (expressed as  $J$ ) can be varied depending upon the distance between conducting planes and neighboring magnetic anions. As a continuous effort to understand the  $\pi\text{-}d$  interaction in charge transfer salts, we have investigated a temperature-pressure ( $TP$ ) phase diagram and magnetoresistance of  $\beta\text{-(BDA-TTP)}_2\text{MBr}_4$  ( $M=\text{Fe, Ga}$ ). The clamped pressure cells made of either BeCu or MP35N alloy developed in NHMFL were used in this study. SCM II and Cell 12 magnet were used to measure high field magnetoresistance.

The  $TP$ -phase diagram of  $\beta\text{-(BDA-TTP)}_2\text{MBr}_4$  is insensitive to the existence of magnetic anions and more or less similar to that of  $\beta\text{-(BDA-TTP)}_2\text{MCl}_4$  ( $M=\text{Fe, Ga}$ )<sup>1</sup> as shown in Fig. 1 (a). As the temperature is decreased,  $\beta\text{-(BDA-TTP)}_2\text{MBr}_4$  undergoes metal

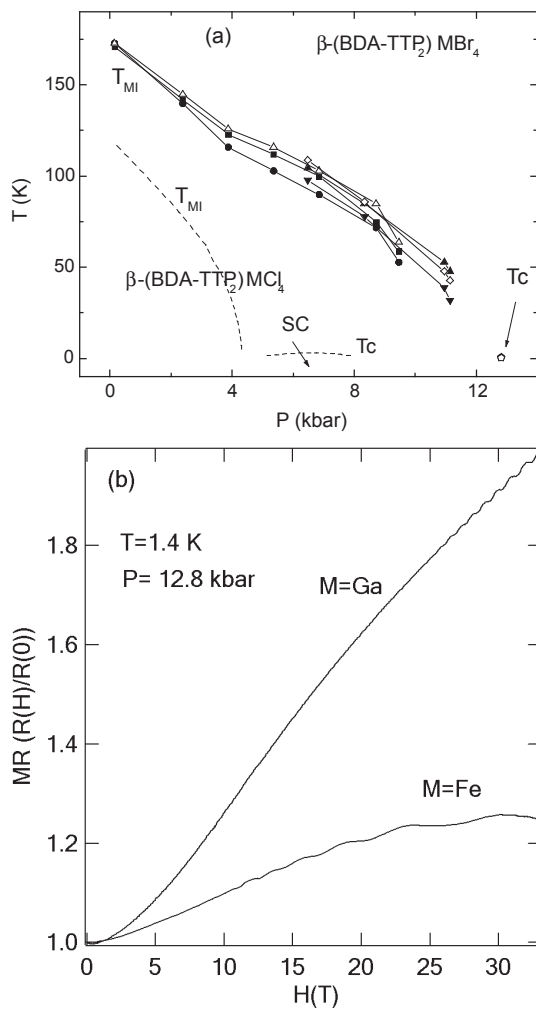


**Figure 1.** (a) The  $TP$ -phase diagram of  $\beta$ -(BDA-TTP)<sub>2</sub>MBr<sub>4</sub> (M=Fe, Ga). Each symbol represents different samples with filled symbols for M=Fe and unfilled symbols for M=Ga. The dashed lines are phase boundaries for  $\beta$ -(BDA-TTP)<sub>2</sub>MCl<sub>4</sub> compounds. (b) MR ( $R(H)/R(0)$ ) of  $\beta$ -(BDA-TTP)<sub>2</sub>MBr<sub>4</sub> at 1.4 K at 12.8 kbar. The SdH oscillation is also observed from for both samples with similar FFT frequency of 900 T. A slow oscillation with frequency of 100 T is observed only for M=Fe sample.

to insulator transition at  $T_{MI}$ . The insulating phase is suppressed with pressure and the superconductivity eventually appears at 12.8 kbar with  $T_{c\text{onset}} \sim 0.5$  K for both M=Fe and Ga samples. Compared to  $\beta$ -(BDA-TTP)<sub>2</sub>MCl<sub>4</sub>, the pressure for  $T_{MI}$  and  $T_c$  shifts to higher values for  $\beta$ -(BDA-TTP)<sub>2</sub>MBr<sub>4</sub>, which may be due to the higher negative chemical pressure effect for the larger MBr<sub>4</sub> anion.

It is of note that both M=Fe and Ga samples show positive magnetoresistance (MR) with small differences between them as shown in Fig. 1 (b). This behavior is rather unusual compared to other organic conductors with local magnetic moments which show negative MR. It is speculated that the  $\pi$ -d interaction in this compound can be much smaller than others. In a simple picture that the interaction is proportional to the extent of overlap between the energy levels of donors and anions, one may need higher pressure to observe the effect of the  $\pi$ -d interaction in this compound.

## Acknowledgements

This work is supported by NSF-DMR 0203532.

## References

- Choi, E.S., *et al.*, *Phys. Rev B*, **70**, 024517 (2004).

**The works by Yong *et al.* and Gervais *et al.* concern novel, crystalline states of electrons confined in two-dimensional systems in semiconductors. These two dimensional electron systems are also known for exhibiting the quantum Hall effects. The reports present examples of advanced, nonstandard rf techniques applied to high magnetic field research. Yong *et al.* employed transmission line-based spectroscopy to a newly discovered electron crystal that exists at high magnetic field. They found this phase, even though strongly affected by disorder, has a correlation length of 80  $\mu\text{m}$  or more. Gervais *et al.* used NMR, detected by changes in resistance on application of rf, to find evidence for a crystal of Skyrmions, exotic particles that bundle multiple electron spins, which occur under certain conditions in 2D electron systems in high magnetic field.**

## Pinning Mode Dispersion of 2D Wigner Solid Phases in High Magnetic Field

Yong P. Chen, R.M. Lewis (NHMFL and Princeton); L.W. Engel (NHMFL); D.C. Tsui (Princeton); L.N. Pfeiffer and K.W. West (Lucent Bell Labs)

The ground state of a sufficiently clean two-dimensional electron system (2DES) in high magnetic field (above the termination of the fractional quantum Hall state series) is generally believed to be a Wigner solid (WS). Pinned by disorder, such a solid is an insulator and possesses a characteristic pinning mode resonance, due to the solid oscillating within the pinning potential. Recent measurements<sup>1</sup> on very low disorder 2DES realized in GaAs/AlGaAs quantum



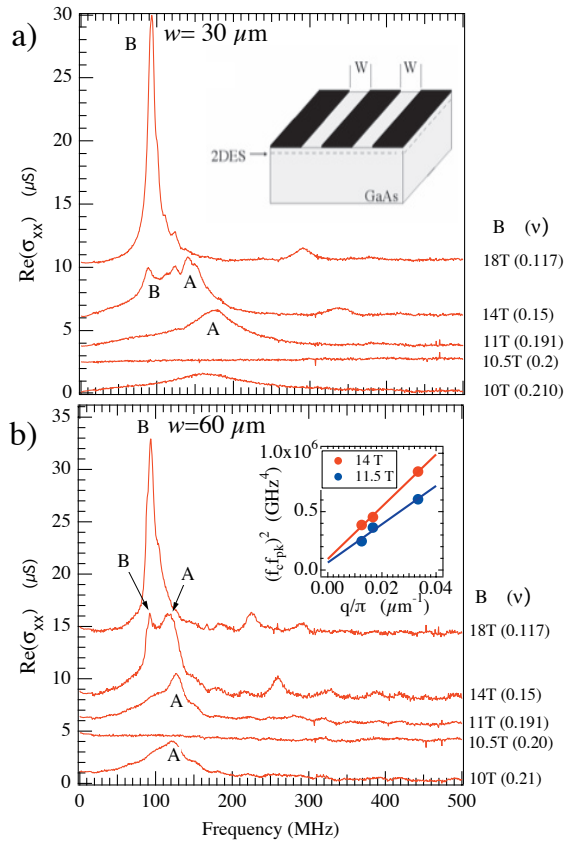


**Figure 1 (a) and (b).** Conductivity spectra for samples with different transmission line widths,  $w=60$  and  $30 \mu\text{m}$ , for various Landau level filling factors  $\nu$ . Resonances interpreted as due to solids A and B are marked. There is a crossover from the A to the B resonance as  $\nu$  decreases. The density of both samples was  $5.1 \times 10^{10} \text{ cm}^{-2}$ , and the measuring temperature was  $50 \text{ mK}$ . The higher frequency peaks may be due to spatial harmonics.

Inset in (a): magnified cross section of transmission line pattern fabricated on top of sample. The transmission line has three conductors, two grounded side planes and a driven center conductor, separated by slots of width  $w$ .

Inset in (b): Experimentally measured dispersion of solid-A pinning mode at two representative magnetic fields. Solid lines show fits to the theory in.<sup>2</sup> Fit parameter was density:  $5.1 \times 10^{10} \text{ cm}^{-2}$  (14.5 T data, red),  $4.9 \times 10^{10} \text{ cm}^{-2}$  (11.5 T data, blue).  $f_c$  is the cyclotron frequency;  $f_{pk}$  is the measured resonance frequency.

## EVIDENCE FOR SKYRMION CRYSTALLIZATION FROM NMR RELAXATION EXPERIMENTS

G. Gervais (Columbia U. and NHMFL), H.L. Stormer (Columbia U.), D.C. Tsui (Princeton), P.L. Kuhns (NHMFL), W.G. Moulton (NHMFL), A.P. Reyes (NHMFL), L.N. Pfeiffer (Lucent), K.W. Baldwin (Lucent) and K.W. West (Lucent).

### Introduction

In the presence of a strong perpendicular magnetic field, the orbital motion of electrons confined to a two-dimensional plane is quantized into discrete Landau levels. When only the lowest of such level is almost completely occupied, the elementary excitations of the system become large topologically stable spin texture known as Skyrmions.<sup>1</sup> Here, we present an extensive study of nuclear magnetic resonance (NMR) spin-lattice relaxation rate in the first Landau level of an extremely high-quality GaAs/AlGaAs sample. We find strong and enhanced relaxation in the limit of  $T \rightarrow 0$  and  $R_{xx} \rightarrow 0$  where localization of electronic states occurs. This is consistent with the predictions of, and finds a natural interpretation in terms of a magnetic ground state containing a Skyrme crystal.<sup>2</sup>

wells found two different resonances, with one crossing over to the other as Landau filling factor ( $\nu$ ) is reduced, suggesting that there are two different solid phases (“A”, dominant at high  $\nu$  and “B”, dominant at low  $\nu$ ).

We have probed the dispersion of the pinning mode of solid A by varying the wave vector  $q=\pi/w$  imposed by a planar transmission line that couples to the 2DES in these measurements, as shown in the inset in Fig. 1a. Samples were made from the same wafer (with 2DES in a  $65 \text{ nm}$  wide quantum well), but with various  $w$ 's ranging from  $20$  to  $80 \mu\text{m}$ . Fig. 1 shows that the peak frequency of the pinning mode ( $f_{pk}$ ) of solid A is lower for larger  $w$ . This trend continues at least to  $w=80 \mu\text{m}$ , the largest  $w$  we measured. This means solid A has some type of correlation length exceeding  $\sim 80 \mu\text{m}$ . The  $q$  dependence of the peak frequency, shown in the inset in Fig. 1b, is in reasonable agreement with the predicted dispersion<sup>2</sup> for the magnetophonon mode of a disorder-pinned Wigner crystal. In contrast, the resonance in solid B is independent of  $w$ .

### Acknowledgements

We acknowledge support from the AFOSR and from the NHMFL in-house research program.

### References

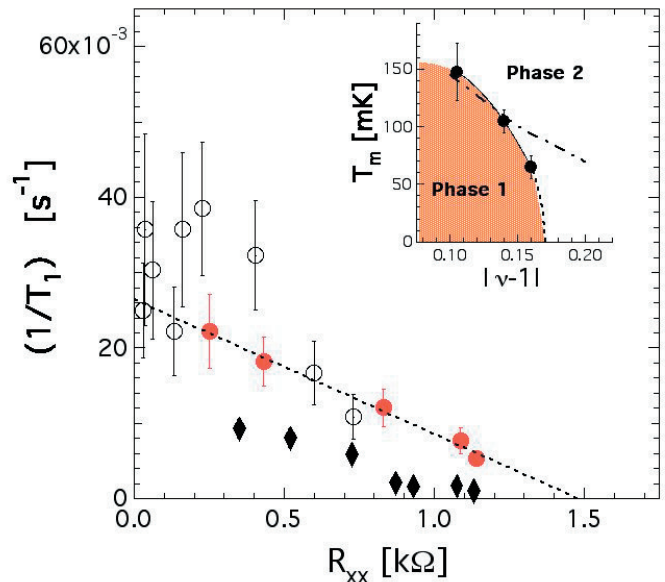
- Chen, Yong P., *et al.*, *Phys. Rev. Lett.*, **93**, 206805 (2004).
- Normand, B.G.A., *et al.*, *Phys. Rev. B*, **46**, 3920 (1992).

## Results and Discussion

Figure 1 shows the spin-lattice relaxation rate ( $1/T_1$ ) extracted using resistively detected NMR in the vicinity of the  $\nu = 1$  Quantum Hall state, at filling factors  $\nu = 0.84$  (diamonds), 0.86 (filled circles), and 0.895 (open circles). The nuclear spin of  $^{75}\text{As}$  is found to relax much more efficiently with  $T \rightarrow 0$  and when a well developed quantum Hall state with  $R_{xx} \sim 0$  occurs. The data show a remarkable correlation between the nuclear spin relaxation and localization. Extrapolating the rate in Fig.1 to the x-axis defines a resistance  $R_m$  at which  $T_1 \rightarrow \infty$ . While there will remain other, weaker relaxation mechanisms, this extrapolated  $R_m$  should provide a measure where nuclear relaxation by the strong low-temperature mechanism ceases. When translated to  $T_m$  via our  $R_{xx}$  vs.  $T$  calibration, the  $T_m$ 's define a temperature boundary for the low-temperature magnetic phase as shown in the inset of Fig.1 vs. the partial filling factor,  $|\nu - 1|$ . Efficient relaxation of the nuclear spins requires magnetic fluctuations in their environment and the data in Fig.1 requires an increase of such fluctuations as  $R_{xx}$  (and hence  $\sigma_{xx}$ ) decreases. A spin-polarized two-dimensional Fermi gas is extremely inefficient in providing such fluctuations. On the other hand, a spin-wave Goldstone mode of a Skyrme crystal<sup>2</sup> provides a very efficient mechanism for relaxing the nuclear spins. Within this scenario, phase 1 would correspond to a square lattice phase of Skyrmions with long-range positional and orientation order, while phase 2 would correspond possibly to a melted skyrmion phase with quasi long-range magnetic order only.

## Conclusions

In the vicinity of the  $\nu = 1$  quantum Hall state, in GaAs/AlGaAs the nuclear spin relaxation increases strongly as the temperature is lowered and when  $R_{xx} \rightarrow 0$ . This strongly suggests that the localized states are responsible for the fast nuclear relaxation. We find a natural interpretation of our data in terms of a magnetic phase of



localized skyrmions relaxing the nuclear spin via a Goldstone mode of the crystal and deduce a partial phase diagram in the  $T$ - $\nu$  plane.

## Acknowledgements

Research funded by the NSF under grant # DMR-0084173 and # DMR-03-52738, and by the DOE under grant # DE-AIO2-04ER46133.

## References

- 1 Sondhi, S.I., *et al.*, *Phys. Rev.*, **B47**, 16419 (1993).
- 2 Cote, R., *et al.*, *Phys. Rev. Lett.*, **78**, 4825 (1997).
- 3 Gervais, G., *et al.*, *Phys. Rev. Lett.*, **93**, 266804 (2004).

**Congratulations to Yoon Lee, Jian-Sheng Xia and Carlos Vicente, all from the NHMFL High B/T facility, for their article titled "A1 and A2 Transitions in Superfluid  $^3\text{He}$  in 98% Porosity Aerogel" in *Physical Review Letters* [Choi, *et al.*, **14**, 145302 (1 Oct 2004)]. This work, performed at the NHMFL's High B/T Facility and partially funded by the In-House Research Program, reports the discovery of the third superfluid phase in helium-three in the presence of high porosity aerogel. The discovery of superfluidity in helium-three was awarded the 1996 Nobel Prize in Physics. This work studies the effects of disorder in this unconventional (p-wave) superfluid by placing the helium-three in 98% porosity aerogel. The newly discovered phase is only observable in magnetic fields above 3 T and at extremely low temperatures below 2 mK. This work maps the high field phase diagram of helium-three in aerogel up to 15 T.**

## OBSERVATION OF A HIGH FIELD PHASE IN SUPERFLUID $^3\text{He}$ IN 98% POROSITY SILICA AEROGEL

H.C. Choi, A.J. Gray (UF, Physics), C.L. Vicente, J.S. Xia (NHMFL, UF), G. Gervais, W.P. Halperin (Northwestern, Physics & Astronomy), N. Mulders (U. of Delaware, Physics), and Y. Lee<sup>1,2</sup> (UF, Physics)

## Introduction

Superfluid  $^3\text{He}$  in high porosity aerogel is the system in which the effects of static disorder on a p-wave superfluid can be investigated in a systemic manner. The nano-meter scale structure of high porosity



aerogel provides a self-sustaining matrix of dilute static impurity which interferes with the formation of Cooper pairs in superfluid  $^3\text{He}$ . The fragile nature of the p-wave Cooper pairs against impurities was clearly demonstrated by the significant depression of the superfluid transition. To date, two distinct superfluid phases have been observed in this system in moderate magnetic fields ( $< 8$  kG). We report our finding of the third superfluid phase in 98% porosity aerogel which appears only in the presence of strong magnetic fields.<sup>1</sup>

## Experimental

We performed continuous wave shear acoustic impedance measurements on both bulk liquid (pure) and liquid in aerogel (dirty) in the presence of magnetic fields up to 15 T at 28.4 and 33.5 bar using the High B/T Facility. In brief, we detect the change in electrical impedance of an ac-cut quartz transducer in contact with both pure and dirty liquid. The acoustic measurement is performed at 8.7 MHz. Temperature is determined by the  $^3\text{He}$  melting pressure thermometer attached right below to the main sample cell made out of pure silver and titanium. In high magnetic fields ( $3 \text{ T} < H < 14.5 \text{ T}$ ), the recent calibration by a University of Tsukuba group was employed.<sup>3</sup>

## Results and Discussion

Fig. 1 shows the field dependent transition temperatures at 28.4 bar. Open (closed) circles are for bulk (aerogel) transitions. The transition features are identified as distinct steps (bulk) and slope changes (aerogel) in the acoustic trace. The single transition feature at zero field splits into two transitions in magnetic fields inducing a new phase appearing inside the wedge. The size of the splitting is linear in field as demonstrated in the figure. The high field phase in bulk has been identified as the  $A_1$ -phase in which only the spin up component participates in forming Cooper pairs. Similar behavior is observed for 33.5 bar. We could not resolve or identify the splitting in aerogel below 3 T. This might suggest antiferromagnetic exchange between the localized  $^3\text{He}$  adsorbed on the aerogel surface and mobile  $^3\text{He}$  spins in liquid.

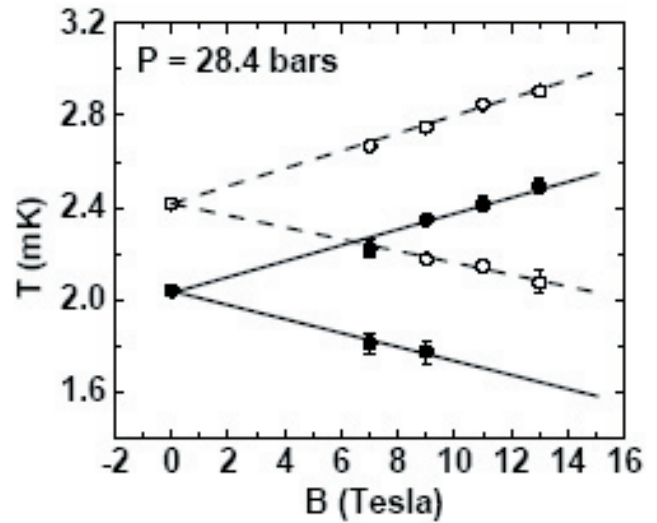


Figure. 1. Transition temperature vs. field

## Conclusions

We observed the superfluid transition in 98% aerogel split into two transitions in the presence of magnetic fields above 3 T at 28.4 and 33.5 bar. The field dependence of each transition is consistent with that of the  $A_1$ -phase observed in pure liquid.

## Acknowledgements

This work is partially supported by a NHMFL IHRP grant and the NSF through DMR-0239483. YL is an Alfred P. Sloan Research Fellow.

## References

- 1 Choi, H.C., *et al.*, *Phys. Rev. Lett.*, **93**, 145302 (2004).
- 2 Fukuyama, H., *et al.*, *Physica (Amsterdam)*, **329B**, 1560-1565 (2003).

# 10 Years of Florida-Bitter Magnet Technology

*M.D. Bird, NHMFL*

10 years ago, on March 18, 1995 the world's first Florida-Bitter magnet (Figures 1 and 2) successfully reached its design field of 30 T at the NHMFL in Tallahassee, Florida. This magnet marked a world record, and with it, a major milestone in the development of resistive magnet technology. It showed that the NHMFL had taken leadership on an international scale by generating much higher fields with resistive magnets than the other magnet laboratories, and was even competing successfully with their sophisticated hybrid magnets. The new technology, invented and developed to technical maturity at the NHMFL, has demonstrated its superiority. It has since become the international standard for high-field dc systems, adopted by most of the world's large dc field facilities.

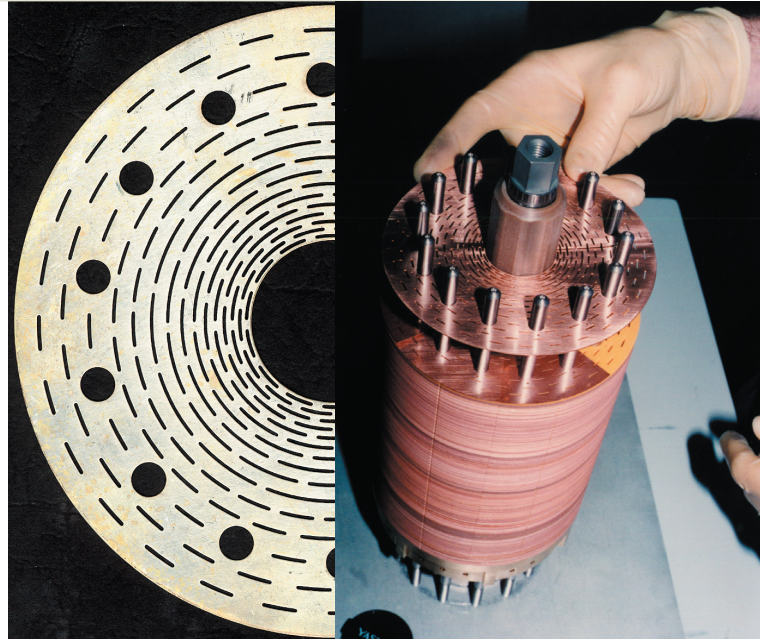


**Figure 1.** Conductor from first Florida-Bitter magnet, 30 T, 1995, NHMFL. Note heavily elongated cooling holes in a staggered grid.

**Figure 2.** Stacking the innermost coil of first Florida-Bitter magnet, 30 T, 1995, NHMFL.

On the road to higher fields, there were historically competing requirements the magnet designer would address: high-field magnets require high current densities that result in (a) high power densities and (b) high Lorentz body-forces. Introducing cooling holes introduces stress and current density concentrations that further raise stresses and power densities. Stronger materials typically have lower electrical conductivity, hence require more cooling holes. Magnet designers worldwide would trade-off strength versus conductivity and cooling.

At the time of the founding of the NHMFL in 1990, two of the most prominent high-field dc magnet labs were the FBNML at MIT in Cambridge, Massachusetts and the GHMFL\* in Grenoble, France. Both labs used the traditional Bitter magnet technology first employed by Francis Bitter in 1936.<sup>2</sup> This technology had two major limitations, both of which were of a mechanical (or structural) nature. First, the mechanical stress in a high-performance disk was typically not uniform but was concentrated at the inner edge by a process called “radial force transmission”. Second, the slits in the disks introduced stress concentrations. These two phenomena limited the peak fields attainable with 10 MW of power, the standard at that time.<sup>1</sup>

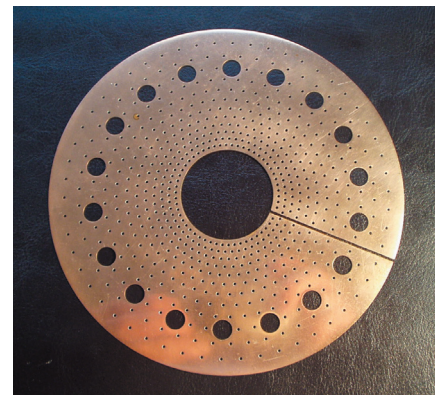


**Figure 3.** Bitter disk from 27 T magnet, 1994, NHMFL. Note round cooling holes.

Consequently, both the FBNML and the GHMFL used more advanced technology for the innermost coils of their highest-performance magnets. The FBNML used radial-Bitter and monohelix magnets that had higher cooling efficiency and were less sensitive to plastic deformation than traditional Bitter magnets. This allowed them to employ higher strength (and lower conductivity) materials and run them into the plastic regime. The GHMFL used the polyhelix technology that eliminated radial force transmission and stress concentrations and allowed more precise optimization than traditional Bitter magnets. This enabled them to use higher conductivity (and



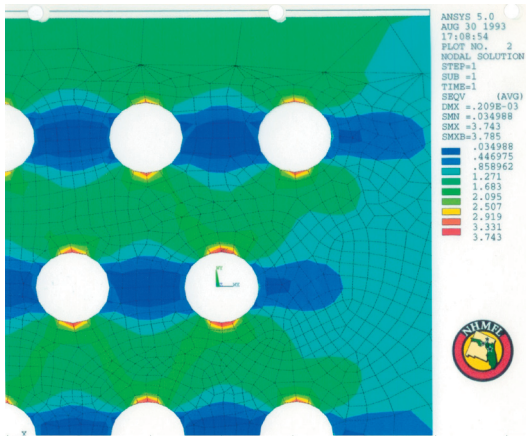


**Figure 4.** Stress distribution associated with round cooling holes. Peak value 3.7 times remote tension.

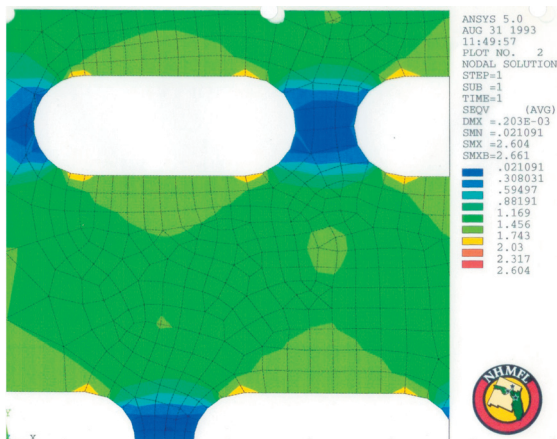


**Figure 5.** Stress distribution associated with elongated cooling holes. Peak value 2.0 times remote tension.



lower strength) materials and operate in the elastic regime with long fatigue life.

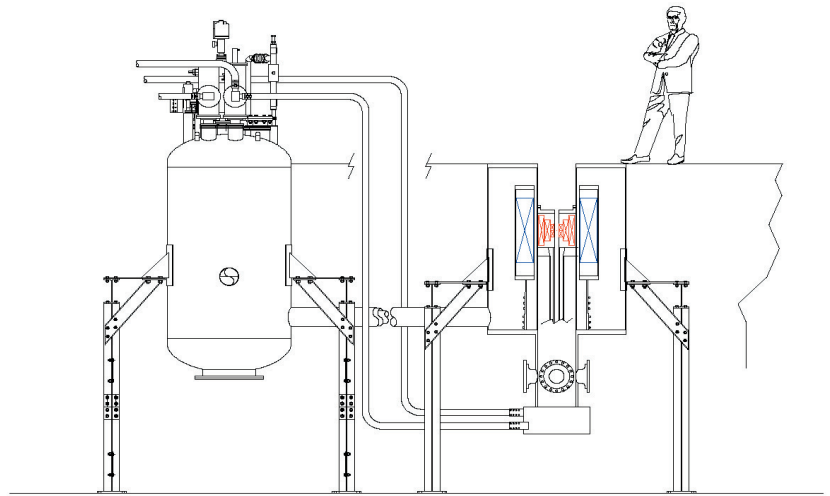
When initiating the development of resistive magnets at the NHMFL, we needed to build a shop, hire and train personnel, create a supply chain, and deliver the first reliable working system in about a year and a half. We decided the first magnet would use the simple, reliable Bitter magnet technology, but we fully intended to develop better technology for future systems. As we were designing the conductors for this first magnet, it was clear that greater efficiency could be attained by optimizing the shape and positioning of the cooling holes.<sup>3,4,5</sup> Time constraints and cost concerns, however, led to the design shown in Figure 3 employing traditional, round cooling holes.

In developing the second magnet at the NHMFL, more attention could be devoted to improving the magnet technology. Figures 4 and 5 present stress contours for two different arrays of holes with remote uni-axial tension. Figure 4 represents a hole-pattern very similar to that used in the 27 T magnet. We see that the peak stress near a hole is 3.7 times the maximum remote tension. Figure 5 represents a hole-pattern that uses the same hydraulic diameter and space factor but, by using elongated holes, the peak stress is only 2.0 times the maximum remote tension.<sup>5</sup> Thus, by employing heavily elongated cooling holes, peak stresses can be reduced by nearly 50%.

In addition, if one employs heavily elongated cooling holes in a Bitter magnet, the way one chooses to arrange those holes can also have a dramatic effect on the overall stress state in the coil. By staggering the consecutive rings of cooling holes, the various rings of conductor become nearly mechanically independent of each other. This drastically reduces the radial force transmission, similar to the independent coils of a polyhelix magnet. The resulting design using highly elongated holes in a staggered grid is called a Florida-Bitter magnet and results in average stresses as low as half that of a traditional Bitter magnet.<sup>6</sup> Indeed, the stress in a Florida-Bitter disk can be as much as 22% lower<sup>1</sup> than that in a (hypothetical) disk without any cooling holes at all!

**Figure 6.** 45 T Hybrid: device, insert disks, and a few of the personnel.

**Figure 7.** Schematic of proposed Series-Connected Hybrid at NHMFL. Resistive insert will employ Florida-Bitter technology.



Thus, with the Florida-Bitter technology, we reject the logical “or” and embrace the illogical “and”. We choose both effective cooling and low stress!

In addition, the technology leads to high-field magnets consisting of a few stacks of identical disks. Each stack can operate within the elastic regime resulting in a long lifetime. This

combination of mass-produced parts operating at modest stress levels results not only in exceptional performance, but also in low life-cycle costs.

Since its introduction in 1995 at the NHMFL, the Florida-Bitter technology has been adopted by four of the five largest dc field facilities worldwide. In addition to six designs in Tallahassee, the NHMFL developed a 30 T magnet for the Tsukuba lab in 1997 and some 33 T magnets for the Nijmegen lab in 2003.<sup>1</sup> In addition, the Sendai lab developed their own hybrid insert using Florida-Bitter technology achieving 30 T in 1999.<sup>7</sup> Finally, the Tsukuba lab completed two Florida-Bitter hybrid inserts (32 and 52 mm bores) in 1999 reaching a record dc field of 37.3 T.<sup>8</sup>

Presently, there are three new Florida-Bitter magnets being fabricated at the NHMFL. A 32 T, 50 mm magnet should be complete in April 2005. A 35 T, 32 mm system is due in the third quarter of 2005 and a 28 T, 32 mm system with high homogeneity is due in the fourth quarter of 2005.

Furthermore, a split resistive magnet is in development at the NHMFL that will likely employ the Florida-Bitter technology, or a new variation thereof. Finally, in July 2004 the NHMFL received funding for the first phase of a new Series-Connected Hybrid magnet project that will employ the Florida-Bitter magnet technology for the resistive insert (Figure 7).

The continuing success of the Florida-Bitter magnet technology is the product of a team of very talented, highly-motivated people, too numerous to list here, who were recruited to the NHMFL by Jack Crow, Hans Schneider-Muntau, and others. The author is greatly indebted to the various persons who have contributed to the success of the program. The author also gratefully acknowledges the editorial comments provided by Hans Schneider-Muntau and Kathy Hedick.

\*The GHMFL did not officially adopt this acronym until a few years later.

<sup>1</sup> M. D. Bird, *Superconductor Science and Technology*, vol. 17, no. 8, pp. R19-R33.

<sup>2</sup> F. Bitter, *Proc. Int. Conf. On High Magnetic Fields* (Cambridge, MA: MIT Press), 1962, pp. 85-99.

<sup>3</sup> G. Kolosoff, doctoral dissertation, Dorpat, 1909, see also paper in *Z. Math. Physik*, vol. 62, 1914.

<sup>4</sup> G. P. Cherepanov, *PMM*, vol. 38, no. 6, 1974, pp. 963 – 979.

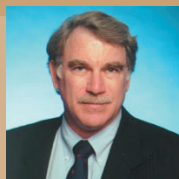
<sup>5</sup> M.D. Bird, *et al.*, *IEEE Trans. On Magn.*, vol. 32, no. 4, 1996, pp. 2444 – 2449.

<sup>6</sup> B.J. Gao, *et al.*, *IEEE Trans. On Magn.*, vol. 32, no. 4, 1996, pp. 2503-2506.

<sup>7</sup> M. Motokawa, *et al.*, *IEEE Trans. On Appl. Supercond.*, vol. 10, no. 1, March 2000, pp. 905 – 908.

<sup>8</sup> T. Kiyoshi, *et al.*, *Physica B* 294-295 (2001) 535-540.

# PEOPLE IN THE NEWS



ALAN G.  
MARSHALL

**Alan G. Marshall**, Kasha Professor of Chemistry & Biochemistry and Director of the NHMFL Ion Cyclotron Resonance Program, has been selected to receive the 2004 Southern Chemist Award. Awardees “must have worked in the South at least 10 years . . . and brought recognition to the South through their work.” Sponsored by the American Chemical Society Memphis Section, the geographic range of the award includes Alabama, Arkansas, North and South Carolina, Florida, Georgia, Louisiana, Mississippi, and Virginia. Marshall is the fourth F.S.U. chemist to win this 52 year-old award, following Greg Choppin (1971), Michael Kasha (1974), and Earl Frieden (1987). The award was presented in Memphis at a banquet on December 9, 2004.

## 2004 American Physical Society Fellows

**American Physical Society Fellowships recognize members who make “outstanding contributions to physics.”** The APS Fellowship Program was created to recognize members who have made advances in knowledge through original research and significant contributions to the application of physics to science and technology. Only half of 1% of the total APS membership is selected for Fellowship in the Society each year.



PETER  
HIRSCHFELD

**Peter Hirschfeld**, Professor of Physics at University of Florida, received his Ph.D. from Princeton. He received the Friedrich Bessel Prize of Alexander v. Humboldt Foundation in 2001. His research interests include superconductivity and correlated electron systems. His citation reads: “*For distinguished contributions to the theory of disordered unconventional superconductors which helped identify d-wave pairing in the high-temperature superconductors.*”



JOHN  
SINGLETON

**John Singleton**, Technical Staff Member at Los Alamos National Laboratory, received his M.A. and Ph.D. in Physics from Oxford University in the United Kingdom. He was co-recipient of the 1998 Daiwa-Adrian prize and first came to LANL in 2000. His research seeks new types of materials for future electronic devices, as well as novel materials and processes that could improve radios or other signal transmitting equipment. His citation reads: “*For elucidation of many-body and reduced-dimensionality effects in molecular organic crystals and semiconductor systems, featuring creative use of optical and magnetic field techniques and clear technical exposition.*”

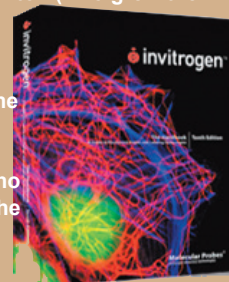


NAI-CHANG  
YEH

**Nai-Chang Yeh**, Professor of Physics at California Institute of Technology and member of the NHMFL External Advisory Committee, received her B.Sc. from National Taiwan University and her Ph.D. from the Massachusetts Institute of Technology. She experiments in superconductivity, magnetism and other strongly correlated electronic systems; scanning probe microscopy; nano-science/technology; low-temperature phases of helium; and development of superconducting cavity-stabilized oscillators. Her citation reads: “*For her contributions to the understanding of cuprate superconductors, vortex dynamics and phase transitions of extreme type-II superconductors, and physical properties of ferromagnetic perovskite oxides.*”

### On the Cover of . . .

The Optical Microscopy Group's images have graced the covers of *Nature*, *Science*, and *Physics Today*. Fluorescence microscopy images, their new initiative on immuno-fluorescence and high-end digital imaging, has been chosen for the cover of the upcoming *Molecular Probes' "Handbook of Fluorescent Products and Research Chemicals."* Special acknowledgements go to Mike Davidson (who leads the group), Nathan Claxton (who grew the cells), Aferdita Ishmaku (who did the staining), and David Homan (who captured the images).





# CONFERENCES & WORKSHOPS

## 5<sup>th</sup> North American FT-ICR MS Conference

<http://www.magnet.fsu.edu/FT-ICR>

April 17-20, 2005

Key West, Florida

Contact: Mark Emmett

[emmett@magnet.fsu.edu](mailto:emmett@magnet.fsu.edu)

850-644-0648

or Karol Bickett

[bickett@magnet.fsu.edu](mailto:bickett@magnet.fsu.edu)

850-644-0535

## Probing Matter at High Magnetic Fields with X-Rays and Neutrons

<http://xraysandneutrons.magnet.fsu.edu/>

May 10-12, 2005

Tallahassee, Florida

Contact: Diane Nakasone

[nakasone@magnet.fsu.edu](mailto:nakasone@magnet.fsu.edu)

850-644-9186



## Electronic Properties of Two-Dimensional Systems and Modulated Semiconductor Structures (EP2DS-16)

<http://ep2ds-16.sandia.gov/>

July 10-15, 2005

Albuquerque, New Mexico

Contact: Diane Gaylord

[ep2ds-16@sandia.gov](mailto:ep2ds-16@sandia.gov)

505-284-2092



## Complex Behavior in Correlated Electron Systems

<http://www.lc.leidenuniv.nl/lc/web/2005/20050801/info.php3?wsid=127>

August 1-18, 2005

Leiden, The Netherlands

Contact: Vlad Dobrosavljevic

[vlad@magnet.fsu.edu](mailto:vlad@magnet.fsu.edu)

850-644-5693

## Physical Phenomena at High Magnetic Fields-V (PPHMF-V)

<http://pphmf5.magnet.fsu.edu>

August 5-9, 2005

Tallahassee, Florida

Contact: Diane Nakasone/Alice

Hobbs

[pphmf5@magnet.fsu.edu](mailto:pphmf5@magnet.fsu.edu)

850-644-9186/644-3665



## 24<sup>th</sup> International Conference on Low Temperature Physics (LT24)

<http://www.phys.ufl.edu/~lt24/>

August 10-17, 2005

Orlando, Florida

Contact: Gary Ihas

[lt24@phys.ufl.edu](mailto:lt24@phys.ufl.edu)

352-392-9244



## International Conference on Ultra-Low Temperature Physics (ULT2005)

<http://www.clas.ufl.edu/ULT2005/>

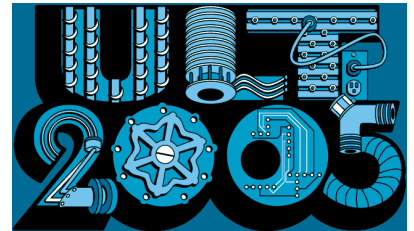
August 11-17, 2005

University of Florida, Gainesville

Contact: Carol Binello

[cbinello@clas.ufl.edu](mailto:cbinello@clas.ufl.edu)

352-392-0780



## Sixth International Symposium on Crystalline Organic Metals, Superconductors, and Ferromagnets (ISCOM 2005)

<http://iscom.magnet.fsu.edu>

September 11-16, 2005

Key West, Florida

Contact: Jim Brooks

850-644-2836

[iscom2005@magnet.fsu.edu](mailto:iscom2005@magnet.fsu.edu)

or Diane Nakasone

850-644-9186



## 8<sup>th</sup> International Symposium on Magnetic Suspension Technology

<http://www.ifw-dresden.de/imw/ISMST8/>

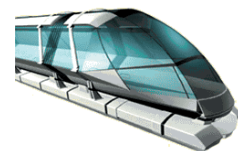
September 26-28, 2005

Dresden, Germany

Contact: Hans Schneider-Muntau

[smuntau@magnet.fsu.edu](mailto:smuntau@magnet.fsu.edu)

850-644-0863





# National High Magnetic Field Laboratory

1800 East Paul Dirac Drive  
Tallahassee, FL 32310-3706  
Tel: 850 644-0311  
Fax: 850 644-8350  
[www.magnet.fsu.edu](http://www.magnet.fsu.edu)



Non-Profit  
Organization  
U.S. Postage  
PAID  
Tallahassee, FL  
Permit No. 55

